

Protection of organic carbon in soil microaggregates via restructuring of aggregate porosity and filling of pores with accumulating organic matter

John F. McCarthy^{a,*}, Jan Ilavsky^b, Julie D. Jastrow^c, Lawrence M. Mayer^d, Edmund Perfect^e, Jie Zhuang^e

^a Center for Environmental Biotechnology, University of Tennessee, 1210 Circle Drive, Knoxville, TN 37996, USA

^b Advanced Photon Source, Argonne National Laboratory, 9700 S. Cass Avenue, Argonne, IL 60439, USA

^c Biosciences Division, Argonne National Laboratory, 9700 S. Cass Avenue, Argonne, IL 60439, USA

^d School of Marine Sciences, Darling Marine Center, University of Maine, Walpole, Maine 04573, USA

^e Department of Earth and Planetary Sciences, University of Tennessee, 1412 Circle Drive, Knoxville, TN 37996, USA

Received 12 October 2007; accepted in revised form 4 June 2008; available online 3 July 2008

Abstract

We examined relationships between the pore structure of microaggregates and the protection of organic matter (OM) within that structure. By using ultra-small angle X-ray scattering (USAXS) before and after combustion of microaggregates at 350 °C, we took advantage of differences in X-ray scattering contrast among soil minerals, OM, and air to evaluate the distribution of the total- and OM-filled porosity within microaggregates (53–250 μm in diameter). Systematic changes in microaggregate structure were observed for long-term field manipulations of land use (a chronosequence of tallgrass prairie restorations) and agricultural management (conventional tillage versus no-till at two levels of nitrogen fertilization). Our results imply that OM preservation arose from the evolution of the architectural system of microaggregates during their formation and stabilization. Soils and treatments with increasing OM in microaggregates were associated with encapsulation of colloidal OM by minerals, thereby creating protected OM-filled pores at the submicron scale within the microaggregate structure. For example, in the prairie chronosequence, microaggregates from the cultivated soil had the lowest concentration of OM, but 75% of the OM that had survived cultivation was in OM-filled pores. Following restoration, the concentration of OM in microaggregates increased rapidly, but the proportion of OM in OM-filled pores declined initially and then increased over time until 90% of the OM was in OM-filled pores. OM totally encapsulated within the pore structure can create spatial and kinetic constraints on microbial access to and degradation of OM. Encapsulation of OM increases the capacity for its protection relative to sorption on mineral surfaces, and comparison of its extent among treatments suggests important feedback loops. The use of USAXS, which has not previously been applied to the study of soil aggregate structures and the distribution of OM within those structures, provided new information on the mechanisms of OM protection in soil microaggregates, and insights relevant to strategies for enhancing carbon-sequestration in soil through changes in agricultural management practices and land use.

© 2008 Elsevier Ltd. All rights reserved.

1. INTRODUCTION

The storage and cycling of soil organic matter (OM) is essential to the functioning of terrestrial ecosystems. For example, soil OM serves as a nutrient reserve and, thus, plays an important role in ecosystem nutrient dynamics

* Corresponding author.

E-mail addresses: jmccart1@utk.edu (J.F. McCarthy), ilavsky-j@aps.anl.gov (J. Ilavsky), jastrow@anl.gov (J.D. Jastrow), lmayer@maine.edu (L.M. Mayer), eperfect@utk.edu (E. Perfect), jzhuang@utk.edu (J. Zhuang).

(Campbell, 1978). It also improves soil structural stability, reduces surface crusting and compaction and increases infiltration, percolation and water holding capacity (Dexter, 1988; Zhuang et al., 2008). Recently, concerns about global climate change have heightened interest in soil OM dynamics, including the effect of warming on existing soil carbon stocks (Conen et al., 2006) and the potential for purposeful enhancement of soil OM sequestration as a strategy to help mitigate anthropogenic carbon emissions (Post et al., 2004).

Soil structure and its dynamics—including the formation, stabilization, and destabilization of aggregates—exert important controls on soil carbon dynamics (Christensen, 2001). Soil aggregate formation, stabilization, and turnover occur through complex interactions of physical processes, chemical associations, and biological activity (e.g., see Oades and Waters, 1991; Tisdall, 1996; Jastrow and Miller, 1998; Six et al., 2004). Processes that bring soil minerals and OM into mutual contact to create the aggregated state—such as wetting and drying, freezing and thawing, root and hyphal growth, plant water uptake, soil faunal activities, tillage and other disturbances—also generate forces that fracture aggregates along planes of weakness depending on the energy of the disruptive force relative to the strength of the mechanisms stabilizing those planes of weakness (Dexter, 1988). Aggregates are stabilized via multiple organic and inorganic mechanisms, with the relative importance and strength of each dependent upon factors such as the spatial scale of the planes of weakness (pores) being bridged, base cation status, clay mineralogy, vegetation type, and environmental conditions (Tisdall and Oades, 1982; Dexter, 1988; Dalal and Bridge, 1996; Jastrow et al., 1998; Six et al., 2004).

In many soils, such as Mollisols and Alfisols, the deposition and transformation of OM is a dominant aggregate stabilizing mechanism, and strong feedbacks exist between aggregate turnover and soil OM dynamics (Oades and Waters, 1991; Dalal and Bridge, 1996; Tisdall, 1996; Feller and Beare, 1997; Jastrow and Miller, 1998; Six et al., 2004). In these soils, aggregate structure is usually hierarchical (Tisdall and Oades, 1982; Oades and Waters, 1991) with primary particles and silt-sized aggregates (<50 μm diameter) bound together to form microaggregates (50–250 μm diameter) and these primary and secondary structures, in turn, bound into macroaggregates (>250 μm diameter). Current evidence suggests that microaggregates are formed inside macroaggregates (Angers et al., 1997; Gale et al., 2000; Six et al., 2000a) and that factors increasing the rate of macroaggregate turnover decrease the formation and stabilization of microaggregates (Six et al., 2000a, 2004). However, microaggregates, and smaller aggregated units, are generally more stable and less susceptible to disturbance than macroaggregates (Tisdall and Oades, 1982; Dexter, 1988).

We focus on microaggregates because it appears that the protection of soil OM against decomposition is greater within microaggregates than macroaggregates (Balesdent et al., 2000; Six et al., 2004). For example, in short-term tracer studies, labeled carbon preferentially accumulated in microaggregates (Besnard et al., 1996; Angers et al., 1997; Gale et al., 2000; Deneff et al., 2001). In laboratory incubation

studies of disrupted aggregates, carbon mineralization is often greater for microaggregates than for macroaggregates (Gregorich et al., 1989; Bossuyt et al., 2002). Furthermore, estimates of the mean residence time of carbon in microaggregates are longer than for the carbon in macroaggregates (Six and Jastrow, 2002).

Many mechanisms have been postulated for the protection of soil OM (e.g., Sollins et al., 1996; Baldock and Skjemstad, 2000; Christensen, 2001). These have been summarized in ways, but one approach (Mayer, 2004) is to categorize them as being due to either organic recalcitrance (e.g., selective preservation, humification) or biotic exclusion (e.g., mineral encapsulation or anoxia). Protection of soil OM within OM–mineral assemblages is generally considered to result from the latter mechanism, wherein OM held among mineral grains excludes either organisms (Kilbertus, 1980) or their enzymes (Mayer, 1994). By its very nature, aggregate hierarchy occurs with a parallel hierarchy of pores that exist between and within aggregates of varying sizes (Elliott and Coleman, 1988). Thus, the smaller pores internal to microaggregates are more likely to exclude biota and their enzymes than those of larger structures.

The goal of this study was to investigate the relationships between microaggregate structure and the sequestration of OM. We focus on the spatial relationships between OM and the pore structure of microaggregates to obtain insights into potential mechanisms responsible for the relatively long residence times for OM in microaggregates, as well as potential strategies to enhance carbon-sequestration in soil. To accomplish this goal, we used ultra-small angle X-ray scattering (USAXS) to investigate the internal pore morphology of microaggregates and the distribution of OM within the microaggregate structure. The evolution of these features were examined in a series of soils representing agronomic management systems that affect carbon accumulation (conventional tillage versus no-till at two levels of nitrogen fertilization), as well as land use options for enhanced carbon storage (conversion of soils from long-term cultivation to perennial vegetation through restoration of native tallgrass prairie).

2. METHODS AND MATERIALS

2.1. Microaggregate sources and preparation

This study focused on two sets of field sites under contrasting agricultural management or land use.

2.1.1. Chronosequence of tallgrass prairie restorations

The study site, located at the National Environmental Research Park at Fermi National Accelerator Laboratory (Fermilab), Batavia, IL, consists of plots in a chronosequence of tallgrass prairie restorations initiated in 1975 on land previously cultivated for over 100 years (Jastrow, 1987, 1996; Allison et al., 2005). Five plots in this chronosequence were sampled in mid-September 2002. A variously cultivated agricultural field was used as the baseline point (time zero) of the chronosequence. In the decade prior to sampling, this field was rotated between maize (*Zea mays*

L.) and soybean [*Glycine max* (L.) Merr.] using conservation tillage and was in maize when sampled. Three restored prairie plots planted in spring 1993, spring 1984, and fall 1978 were completing 10, 19, and 24 growing seasons at the time of sampling. The fifth sampled plot was a remnant of virgin (i.e., never cultivated) tallgrass prairie, which was used to represent the steady-state prairie condition in the chronosequence. Vegetation in the restored and remnant prairies was a mixture of C4 grasses, C3 forbs and sedges, plus a minor C3 grass component. The dominant grasses were big bluestem (*Andropogon gerardii* Vitman) and Indian grass [*Sorghastrum nutans* (L.) Nash]; members of the Compositae contributed significantly to the forb component. All soil samples were taken from areas classified as Drummer silty clay loam (fine-silty, mixed, superactive, mesic Typic Endoaquolls). Replicate soil cores (4.8 cm in diameter; 8 cores for the Virgin Prairie and 6 for the other plots) were taken to a depth of 15 cm from randomly selected locations in each plot, pooled in the field, and refrigerated at 4 °C for one month until the microaggregates were isolated as described below.

2.1.2. Conventional and no-till management systems

The study site, located at the University of Kentucky's Spindletop experimental farm in Lexington, KY, was established to investigate the long-term effects of tillage and fertilization practices on an Alfisol's OM content. The soil is a Maury silt loam (fine, mixed, semiactive, mesic Typic Paleudalfs). Experimental treatments include conventional tillage (CT) versus no-tillage (NT) at two levels of nitrogen fertilization (0 and 336 kg N ha⁻¹) (Frye and Blevins, 1997). The experiment was started in 1970, 32 years before we collected soil from replicate subplots for microaggregate isolation. The site was a bluegrass (*Poa pratensis* L.) pasture for horses for about 50 years before the treatments were established. The treatments are designated as CT0, CT336, NT0, and NT336 to indicate the tillage system and nitrogen fertilization levels. Soil cores (4.8 cm in diameter) were taken to a depth of 15 cm, pooled in the field, and refrigerated at 4 °C for 1 month until the microaggregates were isolated as described below.

2.1.3. Isolation of microaggregates

Field moist soil was gently passed through an 8-mm sieve. Roots, rhizomes, and larger pieces of organic debris were removed during the sieving. When pieces of these materials longer than 8–10 mm passed through the sieve, they were removed manually. The sieved soils were air dried and stored in polyethylene bags at room temperature for 3 months before isolation of microaggregates.

Water-stable microaggregates (53–250 µm) were isolated from the 8-mm sieved soil by using a microaggregate isolator (Six et al., 2000a). For bulk soils, this device isolates microaggregates from within water-stable macroaggregates in addition to collecting any "free" microaggregates external to stable macroaggregates. Briefly, 10 g of air-dry soil were immersed in a column of flowing deionized water maintained at a height of 2.5-cm above a 250-µm mesh screen in the microaggregate isolator and shaken with 50 stainless steel beads (4-mm diameter).

The continuous and steady water flow through the device while shaking caused free microaggregates and microaggregates released from within macroaggregates to be immediately flushed through the screen onto a 53-µm sieve, avoiding further disruption. After all macroaggregates were broken apart, the material caught on the 53-µm sieve was wet sieved for 2 min (50 up-down strokes) to ensure that isolated microaggregates were water stable. Because Fermilab soils exhibit a high level of aggregate stability under perennial vegetation (Jastrow and Miller, 1998), the procedure was modified for these soils to facilitate breakdown of macroaggregates. Thus, air-dry Fermilab soil samples were first slaked by immersion in deionized water in an aluminum pan for 10 min and then subjected to the microaggregate isolator. To collect sufficient amounts of microaggregates for study, 5–8 replicate subsamples of soil from each treatment at each site were processed through the microaggregate isolator and composited. The isolated microaggregates comprised 60–70% of the bulk soil mass for all treatments at both field sites. The isolated microaggregates were transferred from the sieve, dried at 55 °C, and stored at 4 °C in capped glass bottles that were sealed in plastic bags.

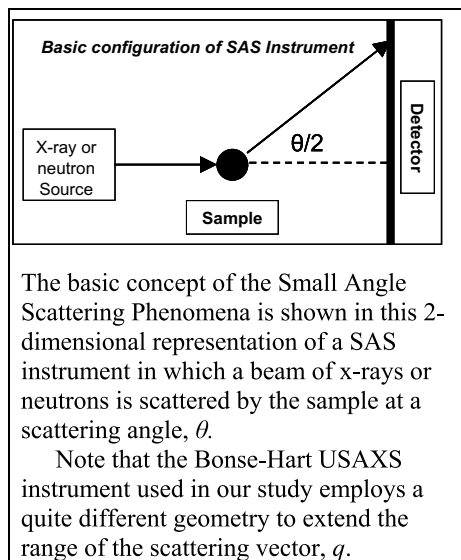
We cannot discount the possibility that drying and storage of soil before rewetting and microaggregate isolation might produce some changes or artifacts compared to soils *in situ*—such as increased flocculation of clay minerals, changes in aggregate stability, shrinkage, formation of microcracks, disintegration of organomineral complexes, and release of dissolved organic carbon (e.g., Bartlett and James, 1980; Kemper and Rosenau, 1984; Dexter, 1988; Peltovuori and Soenne, 2005; Klitzke and Lang, 2007). However, all soils were treated the same, and we consider any resultant effects to be reasonably consistent within each field site. Further, we believe any artifacts induced by drying, storing, and rewetting of soils were minor compared to responses associated with our treatment gradients, and we expect the trends and mechanisms indicated by our results to be minimally affected.

A subsample of the isolated microaggregates for each soil was combusted sequentially at a series of 24-h temperature steps from 250 to 450 °C. The organic carbon content of the intact and combusted samples was measured by using a Shimadzu TOC-V Total Carbon Analyzer in conjunction with a SSM-5000A solid sample combustion unit. No carbonates were detected in the soil samples.

2.2. USAXS data collection and analysis

2.2.1. The small angle scattering phenomena

Ultra-small angle X-ray scattering (USAXS) is the primary tool used here to investigate the size distribution of the pore volume of the microaggregates. The general term, small angle scattering (SAS) refers to the deflection of a beam of radiation (neutrons, X-rays, etc.) from its original direction by interaction with atomic nuclei (for neutron scattering) or electrons (for X-ray scattering) at pore surfaces within the sample (Glatter and Kratky, 1982).



The intensity of the scattered neutrons or X-rays is measured as a function of the momentum transfer, q , which is related to the solid (i.e., three-dimensional) scattering angle, θ , by:

$$q = 4\pi \sin \theta / \lambda \quad (1)$$

where λ is the wavelength of the radiation used. Combining Eq. (1) with Bragg's law, the length scale, L , probed at a given q range follows the general inverse relationship:

$$L \sim 2\pi / q \quad (2)$$

SAS techniques have been applied to study pore structure of a variety of materials such as petrographic samples (Sastry et al., 2000; Radlinski and Hinde, 2001; Radlinski et al., 2004), wood charcoals (Venkatraman et al., 1996), porous alumina (Rasmussen, 2001) and clay minerals (Bihannic et al., 2001). Application of SAS to natural soil systems has focused on characterizing the fractal properties of soil particles, or humic substances extracted from soil (Borkovec et al., 1993; Tombacz et al., 1998; Rice et al., 1999; Diallo et al., 2005). The term "fractal" implies a complex shape that appears similar at all scales of magnification; in SAS, a fractal approach is indicated if scattering curves strictly conform to a monotonic power-law increase in scattering intensity over a very large range in q . We also note that the studies cited above which invoked a fractal structure were instrumentally limited to a narrow q -range and could not rigorously test the strict monotonic power-law criterion for a fractal structure, or chose to limit their analyses to a selected range of q where the fractal criterion did obtain.

We take a non-fractal approach because we found that several of our scattering curves do not strictly conform to a monotonic power-law increase in scattering intensity over the 9 order-of-magnitude range of scattering intensity and the 4 order-of-magnitude range of q accessible using USAXS. Rather, we took an inverse pore size distribution approach to analyze the scattering because, unlike the fractal models, it does not assume any underlying structural

arrangement of the porous medium. It should be noted, however, that the two methods are complementary for materials that exhibit power-law scattering; each describes the same physical microstructure using a different set of parameters. One can loosely compare this to wave- and particle-based descriptions of radiation, both describing the same physical phenomena in different ways. Many natural microstructures exhibit power-law scattering behavior over a limited range of q . For such systems, inverse and fractal analyses are equally meaningful. On the other hand, non-fractal scattering systems cannot be described in fractal terms, making the inverse pore size description method generally more applicable.

The scattering of neutrons or X-rays occurs exclusively at the interface between the solid matrix and a pore space containing material, such as air, that differs substantially in its ability to scatter the radiation. The pattern of scattering intensity, $I(q)$, versus the scattering angle, q , is then determined by the geometry of the pore-matrix interface at various length scales. This pattern can be related to a pore size distribution if the Euclidean shape of the pores is known or can be reasonably assumed. The intensity of scattered radiation is then related to the scatterers' size distribution. For a two-phase scattering system, one can express the intensity of scattering as described by (Kotzias et al., 1987):

$$I(q) = |\Delta\rho^2| \int_0^\infty |F(q,r)|^2 V^2(r) NP(r) dr \quad (3)$$

where $\Delta\rho^2$ is the scattering contrast between the pore and matrix, $F(q,r)$ is the scattering form factor for particulate scatterer shape, $V(r)$ is the volume of sample material within the X-ray or neutron beam, N is the total number of scattering particles, and $P(r)$ is the probability of occurrence of scatterers at size r . The term $V(r)$ is often referred to as the sample thickness because the x - and y -dimensions of the sample are the known shutter settings on the incoming beam. In practice, the known or estimated sample thickness is input in calculation of the sample intensity of scattering ($I(q)$). This formula is, for computational purposes, replaced by a summation formula with a limited number of bins in radii:

$$I(q) = |\Delta\rho^2| \sum_{r_{\min}}^{r_{\max}} |F(q,r)|^2 V^2(r) NP(r) dr \quad (4)$$

Compared with other techniques, SAS has the ability to study a wide range of void sizes (from ~ 10 Å to 15 μm); furthermore, unlike N_2 adsorption or mercury porosimetry, which can examine only that portion of the porosity that the probe molecule can access from the exterior, X-rays and neutrons penetrate throughout the sample. Thus, X-ray or neutron scattering provides information on the entire porosity of a sample. In addition, various materials differ in their ability to scatter X-rays or neutrons, and thus, differences in the composition of material within a pore may result in contrasts in scattering intensity; for example, differences in X-ray or neutron contrast have been used to determine details of porosity development of carbon during heating and solvent swelling (Hall et al., 1997; Antxustegi et al., 1998a,b; Calo et al., 2001).

2.2.2. USAXS instrumentation

USAXS measurements were conducted at the UNICAT beam line of the Advanced Photon Source (APS) at Argonne National Laboratory (Argonne, Illinois, USA). The UNICAT ultra-small angle X-ray scattering instrument utilizes Bonse–Hart double crystal optics to extend the range of the USAXS down to lower scattering vectors. The measured scattering data set is slit-smearred in the horizontal direction, but was numerically desmeared to recover the standard (pinhole-collimated) small angle scattering data. Details of the UNICAT system are described by Long et al. (2000). This instrument uses absolute calibration based on first principles (standard-less), providing results directly on an absolute scale. The wavelength was 1.109 \AA^{-1} with a measurable q -range of 10^{-4} to 10^{-1} \AA^{-1} . USAXS data were corrected and analyzed using a software package “Irena”, developed by our co-Author, Jan Ilavsky for analysis of small angle scattering data. This software can be accessed at (<http://usaxs.xor.aps.anl.gov/staff/ilavsky/irena.html>).

2.2.3. Preparing the microaggregate sample for exposure to the USAXS beam and determining the sample volume (thickness) in the X-ray beam

The microaggregates were prepared for exposure to the USAXS beam by immobilizing them on 1-mm thick Kapton tape, which has a low and stable scattering intensity; empty Kapton “blanks” were measured along with the samples and their scattering spectra subtracted from that of samples. Specifically, the Kapton was taped to a thin plastic square with an ~ 10 -mm hole in the center. The sticky side of the Kapton was attached to cover the hole in the plastic; an excess of microaggregates needed to cover the hole was added and, to promote contact with the tape, the microaggregates were very gently tapped onto the tape using the eraser of a pencil; microaggregates that did not adhere to the tape were poured off and weakly attached microaggregates removed with several flicks of the finger on the under side of the plastic. These strongly attached microaggregates resulted in a sample with an even coating of an approximate monolayer of microaggregates. The samples was protected by a second layer of Kapton tape was placed over the sample. Visually, it was evident that the sample contained voids interspersed with immobilized microaggregates that varied in size, thickness and density. The prepared sample was then transport to the USAXS beamline. The samples were taped the 16-posion sample holder on an x - y linear actuators and positioned in the beam.

Eqs. (3) and (4) specify that calculation of the absolute scattering intensity ($I(q)$) of X-rays requires knowledge of the volume of sample in the beam (Vr); As mentioned after Eq. (3), this term is effectively specified as the sample thickness. We specified a sample thickness of $100 \mu\text{m}$ for calculations of scattering intensity of all samples. This value estimated from the weight-averaged microaggregate diameter from dry sieving of several samples, as well as from an estimate of the relative abundance of voids and solids in the X-ray beam, estimated from radiographs of the samples in the X-ray beam.

In an attempt to further evaluate the sample thickness, we directly visualized the voids and solids in the X-ray beam via a radiogram camera mounted beside the X-ray detector on a linear actuator aligned with the X-ray beam exiting the sample. For a large number of the samples, identical fields-of-view of both the radiogram image and X-ray scattering data were collected within minutes of each other by moving the linear actuator; radiograms and scattering data were numbered to assure proper identification of the two data for each sample. Visual inspection of the radiograms of a very large number of samples revealed a reasonably uniform distribution of solid and voids in radiographs. More quantitative measurement of the solid to void ratio and particle size within the X-ray beam was attempted using computerized image analysis. This approach failed due to the classic problem of defining the threshold of image intensity that differentiated a solid from a void (Sahoo et al., 1988 and references therein).

To obtain a more quantitative evaluation of the magnitude of the variability in thickness among samples, we used the Lambert–Beer Law, which relates the measured sample transmission to the effective sample thickness of the sample material: ($\ln T_m = \mu_p^* t$), where T_m is the measured transmission, μ_p is the linear X-ray attenuation coefficient of the sample and t is the effective sample thickness. The attenuation coefficient was calculated for a mixture of kaolinite and montmorillonite, the predominant minerals in the soil, and the same coefficient was used in calculations for all samples. This alternate method, based on empirical data on the measured X-ray transmission for each sample indicated that samples had approximately the same thickness within a variation of only 8%, although the absolute value of the sample thickness remains an approximation. This approximation should not compromise our scientific goal because our approach does not rely on knowledge of the absolute scattering intensity, but rather focuses on relating patterns of changes in the microaggregate architecture and distribution of OM within the microaggregates from soils with contrasting land use or management histories. The similarity of sample thickness across soils makes all results subject to the same approximation of the absolute value of the sample thickness, and should therefore have a minimal impact on interpretation of the patterns of change observed for different soils and treatments.

Although almost all samples had very similar transmissions, there were a small number of samples that were outliers with very low transmissions. Visual inspect of the radiograph for those samples confirmed that those few samples with anomalously low transmissions also exhibited radiographs that were extremely dense (i.e., X-rays transmission was blocked by the size and/or density of the particles in the sample). These samples were discarded and not used in other calculations or data interpretation.

2.2.4. Data reduction and calculation of size distribution of the pore volume

We estimated the size frequency distribution of voids using the maximum entropy method available within the Irena software (see above). Based on SEM observations of the microaggregates, we used a shape of an oblate

spheroid (aspect ratio of 0.1). The fitting solutions also converged with this shape more readily than with many other shape factors tested, suggesting compatibility of this model with our data. The pore volume distribution (i.e., the relationship between the volume enclosed in a pore and the size or that pore) is presented as a function of the larger dimension of these spheroids. Generally, interpretation of a size distribution from small angle scattering data involves the inversion of an integral equation for which there is no exact solution. Using the size distribution as a histogram, f , it is possible to rewrite the scattering equation as a linear equation.

$$I = Gf, \quad (5)$$

where the matrix component, G , describes the assumed morphology of the scatterers underlying the measured data, I . Solution of the linear scattering equation by a direct matrix inversion is not unique due to the high condition number of G (Potton et al., 1986). Potton et al. (1988) described a method for solution of the linear equation by the maximum entropy method. In short, their *MaxEnt* method maximizes the configurational entropy of the histogram subject to the scattering calculated from that histogram fitting the measured data to within the experimental errors. These two constraints are imposed simultaneously through the use of a Lagrange multiplier. The maximum entropy code implemented in the “Irena” software package is a modification of Potton’s original code by Jemian et al. (1991).

2.2.5. Reproducibility of estimates of the size distribution of pores within microaggregates

The reproducibility of pore volume estimates derived from scattering curves was evaluated by preparing triplicate samples of microaggregates from the same sample container. Each of the replicates was prepared at different times. The microaggregates were derived from four independent site/treatment sources (3 Fermilab ages and one Kentucky treatment). When the samples were taken to the USAXS instrument, each was positioned in different locations on the multiport sample holder. The spectra were obtained at different times, and sometimes different days. The scattering data from the triplicate scattering curves were independently reduced and analyzed in the Irena software to obtain a pore size distribution for each of the triplicates. For each set of triplicates from each of the four soil sources, we calculated the average of the estimated size distribution of total pore volume ($\text{cm}^3 \text{g}^{-1}$ microaggregates) as well as that within the four size classes shown in the insets of Figs. 3 and 4. As a reasonable indication of the reproducibility of our estimates of the size distribution of pore volume, we calculated the standard deviation about the average for the estimated size distribution of pore volume for all samples (12 samples representing the triplicates from the four site/treatment sources). The mean of the cumulative total pore volume for all 12 samples was $0.07 \text{ cm}^3 \text{g}^{-1}$ (microaggregate) with a standard deviation of 0.017 ($<2\%$ of the mean); this suggests that the pore of the volume estimates are highly reproducible. The standard deviations about the estimated individual size distributions of pore volumes for the individual size fractions (shown in

insets in Figs. 3 and 4) were even lower, ranging from 0.003 to 0.006.

2.2.6. Estimation of total and OM-filled porosity in microaggregates from USAXS

Unlike the simple two-phase system (Eqs. (3) and (4)), our system is actually composed of more than two phases: mineral soil, OM-filled voids, and air-filled voids. The system with three components can be too complicated to handle rigorously, so we have decided to treat it approximately as system of two independent scattering populations in dilute limit. The model outcome is, that from such populations, the intensities can be simply summed together. While this is an approximation, it is well accepted and common in small angle scattering applications, especially in materials science. Actually in cases of populations of scatterers with no spatial correlations between the components, and in the dilute limit, summing of intensity is a rigorous solution—(see Chapter 232, pp. 66–68 in Guinier and Fournet, 1955).

An approximation of a dilute system of non-interacting scatterers may not be totally correct for our scattering system; therefore we emphasize the “approximation” in describing this method. Spatial correlations are also unlikely in our system and we have not observed any manifestation of spatial arrangements. For systems with no spatial correlations between the components the interactions between the different phases can be neglected (Guinier and Fournet, 1955). As further justification, it has been found in studies of other materials (ceramics) that systems with broad size distribution of pores can often be treated as dilute systems up to very high volume contents, as they are effectively dilute on any specific length scale.

We should also point out that the method we are using here is really only another application of the contrast matching technique used extensively in small angle neutron studies to analyze multicomponent systems (Avdeev, 2007) or anomalous small angle X-ray scattering studies (Kirby et al., 2007; Lee et al., 2007; Pranzas et al., 2007); each of these studies employed these routinely applied neutron contrast methods. In analyses of multiphase systems with a complicated small angle scattering profile, the contrast of one phase is changed and the difference in scattering data is attributed to the change in the contrast of that phase. This phase is then analyzed using a two-phase approximation. In the present case, we are applying the same method, but the change in the contrast is the result of combustion of the OM-filled voids.

As was the case for the approximation of the absolute sample thickness, the two-phase approximation should not compromise our scientific goal because our approach does not rely on knowledge of the absolute scattering intensity, but rather it focuses on relating *patterns* of changes in the architecture of microaggregate structure affecting OM distribution and preservation for a series of soils representing contrasting agronomic management systems that affect carbon accumulation. Because the results from all soils were subject to the same approximations, they should therefore have a minimal impact on interpretation of the patterns of change observed for different soils and treatments.

We used contrast variations in X-ray scattering from pores filled with OM, compared to scattering from air-filled pores, to determine the pore size distribution of two classes of porosity: (i) the total porosity (defined here as the total volume of pores within and among mineral grains, regardless of whether those pores are occupied by air or OM), and (ii) those pores that are filled with OM. The total porosity was determined using data from microaggregates that were combusted at 350 °C for 24 h to remove the OM (Mayer et al., 2004); the potential impact of combustion on the size distribution of pore is discussed in greater detail below.

Our simplified two-phase system is an approximation of the dilute limit with non-interacting populations of scatterers, for which we can assume that the total scattered intensity $I(q)_{\text{total}}$ changes as a result of OM removal by combustion. $I(q)_{\text{total}}$ before combustion reflects the sum of the scattering in empty mineral pores as well as pores completely or substantially filled with OM (Eq. 6).

$$I(q)_{\text{total before combustion}} = I(q)_{\text{empty mineral pores}} + I(q)_{\text{OM-filled pores}} \quad (6)$$

After combustion (arrow in Eq. (6A)), pores with OM become OM-free empty mineral pores.

$$I(q)_{\text{OM-filled pores}} \rightarrow I(q)_{\text{OM-free empty mineral pores}} \quad (6A)$$

As a result, after combustion, the total scattering curve reflects scattering from both the pores that had originally been empty, as well as from those pores that had originally been completely or substantially filled with OM prior OM removal by combustion (Eq. (6B)).

$$I(q)_{\text{total after combustion}} = I(q)_{\text{original empty pore and those previously filled with OM}} \quad (6B)$$

Thus, the difference curve from subtraction of the scattering curve for combusted sample (mineral matrix) from that for intact sample (mineral matrix + OM) yields an estimate of that fraction of the total porosity completely or substantially filled with OM (Eq. (6C)) (We address the impact of pores that had been only partially filled with OM in Section 2.2.8).

$$I(q)_{\text{OM-filled pores}} = I(q)_{\text{total of combusted sampler}} - I(q)_{\text{total of intact samples}} \quad (6C)$$

The intensity of scattering is proportional to the difference in the scattering power ($\Delta\rho^2$) of the matrix and pore space (Eqs. (3) and (4)). Differences in the scattering intensity (e.g., scattering curves in Fig. 1) can be used to approximate the size distribution of the pore structure and the evolution of the OM-filled pore system of microaggregates isolated from different sites and treatments. Because of the dependence of scattering intensity on the scattering contrast ($\Delta\rho^2$), we can use the difference in scattering contrast between the mineral pores containing OM compared to empty, air-filled voids to approximate the evolution of the size distribution of the total- and OM-filled porosity within the microaggregates using the method below (Eqs. (6–9)).

The effectiveness of a material to scatter X-rays, expressed as a scattering length density (ρ) depends on the abundance and atomic number of the constituent elements

as well as the density of the material. For these samples, the scattering contrast ($\Delta\rho^2$) is the difference in the scattering length density (ρ) of the predominant layer silicate minerals comprising the microaggregate and the air- or OM-filled pore voids. Air is a very weak scatterer of X-rays ($\rho_{\text{air}} = 1 \times 10^2 \text{ cm}^{-2}$), compared to the minerals ($\rho_{\text{mineral}} = 2.2 \times 10^{11} \text{ cm}^{-2}$). The value for ρ_{mineral} was based on the composition and density of the minerals in Fermilab chronosequence soils which are dominated by montmorillonite and kaolinite with smaller amounts of illite and vermiculite. The calculated values of ρ were similar for all these minerals, averaging $2.2 \times 10^{11} (\pm 5 \times 10^9) \text{ cm}^{-2}$. Similar calculations of the ρ_{mineral} for the Kentucky Spindletop site, for which hematite and quartz were important minerals in addition to montmorillonite and kaolinite, established that the ρ_{mineral} was in the same range because the higher ρ for hematite was somewhat counterbalanced by the lower value for quartz. The scattering contrast between the mineral matrix and air void is

$$\Delta\rho^2 = (\rho_{\text{mineral}} - \rho_{\text{air}})^2 \approx (\rho_{\text{mineral}})^2 = 4.8 \times 10^{22} \text{ cm}^{-4} \quad (7)$$

When OM is present in the intact (not combusted) microaggregates, the scattering curve reflects more a complex interaction of the X-rays with multiple pore types, including pores consisting of minerals free of OM, and minerals with OM that fills the pore void or occupies a substantial portion of the pores, and, to a minor extent, minerals with OM coatings in air-filled voids (see below). In the case of the OM-filled void, the contrast between the mineral and OM is

$$\Delta\rho^2 = (\rho_{\text{mineral}} - \rho_{\text{OM}})^2 = 1.2 \times 10^{22} \text{ cm}^{-4} \quad (8)$$

where ρ_{OM} is the scattering length density of the OM, calculated to be $1.1 \times 10^{11} \text{ cm}^{-2}$ based on an average elemental composition of soil organic matter (relative atomic abundances of C:H:O:N of 0.55:0.04:0.4:0.01) and an OM density of 1.3 g cm^{-3} (Adams, 1973; Mayer et al., 2004).

The scattering intensity is substantially greater if an OM-filled pore is emptied due to removal of the OM by combustion (Fig. 1). This change in contrast before and after combustion for the pores originally filled with OM will be used to estimate the pore volume of the OM-filled pore from the difference curve resulting from subtracting the curves before and after combustion. The left side of Eq. (9) is not the contrast of OM-filled pores *per se*, but the change in contrast due to combustion.

$$\begin{aligned} \Delta\rho_{\text{OM-filled}}^2 &= (\rho_{\text{combusted}})^2 - (\rho_{\text{not combusted}})^2 \\ &= (\rho_{\text{mineral}})^2 - [(\rho_{\text{mineral}}) - (\rho_{\text{OM}})]^2 \\ &= 3.6 \times 10^{22} \text{ cm}^{-4} \end{aligned} \quad (9)$$

2.2.7. Impact of combustion on the size distribution of pores

Our approach of determining the size distribution of total and OM-filled porosity by comparison of scattering curves obtained before and after combustion at 350 °C is a source of potential experimental concern. Mayer et al. (2004) presented several arguments and references based on non-SAXS data to indicate insignificant disruption of pore structure by the 350 °C oxidation treatment. This treatment has the potential to change the arrangements

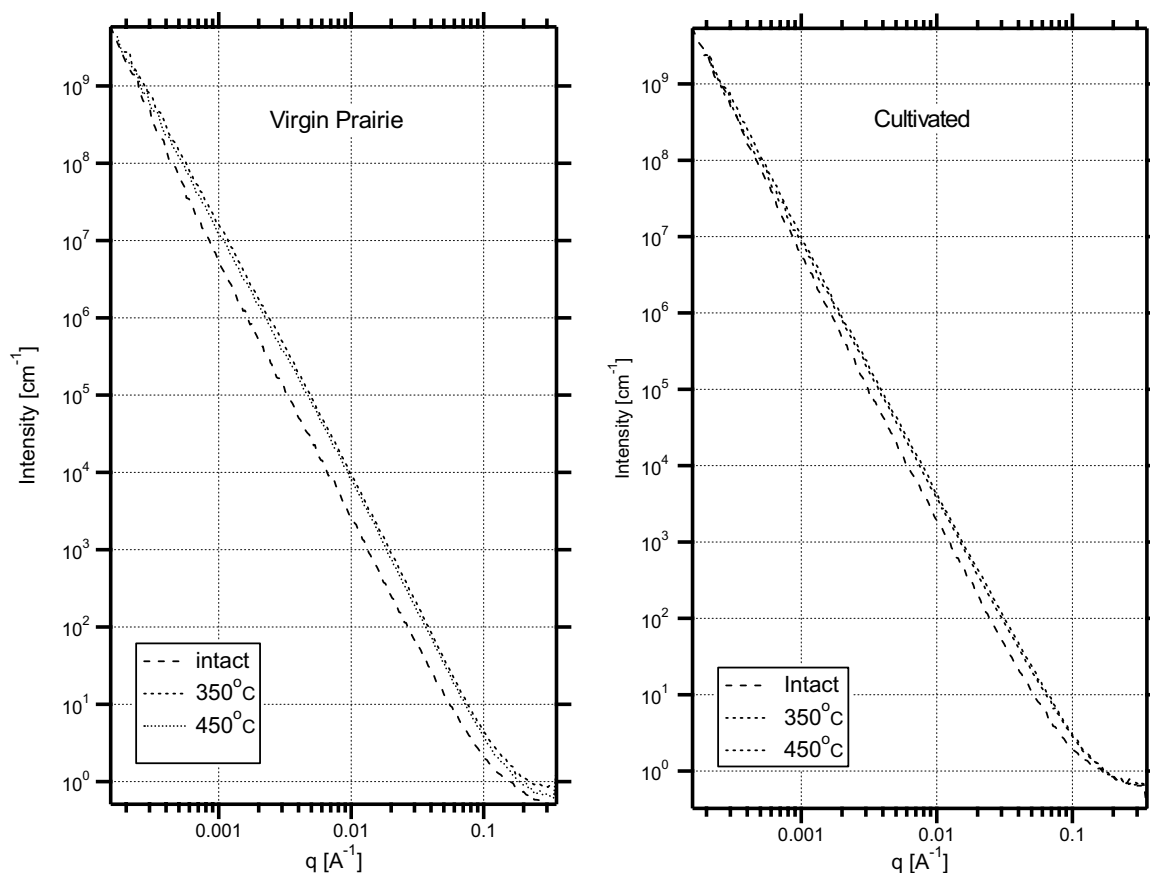


Fig. 1. USAXS scattering curves for microaggregates from the Fermilab Virgin Prairie and cultivated sites are compared for samples that were not combusted (intact) or combusted at 350 or 450 °C (combustion at the higher temperature did not affect the porosity structure). The ordinate is the intensity of X-ray scattering, reflecting the abundance of surface area of pores over a 3 order-of-magnitude range in the size of the scatterers, expressed as a function of the momentum transfer, q , which is inversely related to the length scale of the scatterer (Eq. (2)). The negative slope of the scattering curve indicates that the total surface area of scatterers (intensity) increases with the length scale of the pores. The lower scattering intensity for the intact, compared with combusted, samples is due to the presence of OM-filled pores, which reduces the scattering contrast (Eqs. (3)–(5)); the smaller separation for the Cultivated, compared to Virgin Prairie, reflects the lower abundance of OM-filled pores in microaggregates from Cultivated soil. Although the curves appear to be close on a log–log scale, intensities can differ by factors of 4 or 5, even in closely spaced curves. The scattering curves for OM-filled pores were obtained by subtracting the curve of the combusted samples (minerals, but no OM) from that of the intact (minerals with OM) curves (Eqs. (6) and (6A)). The resultant scattering curve was used to estimate the size distribution of the pore volume for OM-filled pores in these soils (Fig. 3, right panel).

among phyllosilicate grains that form the pores. In that paper, we offered several lines of evidence suggesting that these arrangements, collectively called microfabric, remain largely unchanged after combustion at 350 °C. The USAXS scattering curves in (Fig. 1) indicate that there is no detectable change in the pore structure over 3 orders-of-magnitude in length scales, suggesting that the microfabric is retained after muffling. The scattering curves for the samples combusted at 350 and 450 °C are essentially identical (Fig. 1), indicating that the microaggregate structure is unchanged even at higher temperatures. Carrado and coworkers (Carrado and Xu, 1999; Carrado et al., 2002) also found only small changes in pore size distribution by gas sorption measurements upon muffling of synthetic clay-organic matter systems, which they corroborated using both SAXS data and TEM observations. They argued that the mesopore size pores are controlled by interparticle contacts among clay tactoids or domains (microaggregates of individual clay

crystallites). Indeed, the literature on formation of mesoporous clay catalysts, which relies on using organic templates to create pillared arrangements among clay flakes, routinely uses muffling (“calcination” in that literature) to eliminate the organic templates without loss of mesopore structure (Zhu et al., 2002). Mayer et al. (2004) also found that ultra centrifugation of their samples (47,800g for 30 min) had only a small impact on pore volume distribution, providing further evidence for the robust nature of microfabric in their sediments.

2.2.8. Justification for the term “OM-filled pores”

We use the term “OM-filled pores” to refer to the pores identified from the difference curve resulting in a change in contrast due to combustion (Eq. (9)). However, it is possible that OM fills only a portion of a given pore. Under these circumstances, the estimated size distribution of OM-filled pores could be subject to some inaccuracy. To evaluate

the impact on the estimates of size distribution of the pore volume, consider three basic cases:

1. The volume of OM coating an air-filled pore is much smaller than the void. In this case, the removal of the OM by combustion has little or no effect on the small angle scattering from sample because the mineral material would dominate scattering. The pore scatters at roughly the same q before and after combustion. Thus, there is a minimal effect on our results because the effect on scattering is small and is reflected approximately the same q .
2. OM fills or almost fills the entire pore. This is our default case. The effect of a small fraction of this pore that was not originally filled by OM will result in some error to our results. However, because the size of this unfilled volume is much smaller than the pore size, the effect will happen at significantly larger q values and will result in some distortion of results for small pores. This will occur at the highest q values and any minor distortion will be limited to the small pores.
3. The problematic case is where OM fills about half of the pore volume. Before combustion, the empty space dominates scattering. After removal of the OM by combustion, we now have a larger void with a larger scattering volume. Therefore, some of the scattering intensity at higher q will be lost, and more intensity added at lower q . However, this shift should not have a significant impact on estimates of the size distribution OM-filled pores or on data interpretation. From a practical perspective, we set the size distribution modeling tool in *Irena* to distribute the fitted volume estimates into 400 logarithmically allocated bins, thus further reducing the impact of small shifts of q on the estimated size distribution, especially compared to the three orders-of-magnitude pore size range examined in USAXS. Thus, although the uncertainties discussed above could have some influence the absolute values of the pore volume estimates, there is good evidence that it will have a limited influence on the interpretation of the data, especially with respect to the relative differences in the distributions of total- and OM-filled pores between sample treatments.

The concept of "OM-filled pores" is also confirmed by data in Mayer et al. (2004). Inspection of the pore volumes (measured via nitrogen adsorption) in the soils (Fig. 3b), indicated only small changes in volume before and after combustion for all soils except two with extremely high OM loadings (8% by weight, OC:SFA \sim 5), much higher loadings than in this study. The small changes in volume argue for Case 1 above. Granted, the pore size range is limited, but it seems unlikely that there is enough OM to fill the larger pores.

2.2.9. Nitrogen sorption isotherms

Gas sorption analysis was performed on a Quantachrome A-1 Autosorb, by subjecting samples to varying partial pressures of N_2 gas (UHP grade) at 77 K. All solids were initially degassed in a vacuum oven (150 °C at

50×10^{-3} Torr for 18 h) to remove surface-adsorbed water, followed by a minimum of 3 h at 10×10^{-3} Torr on the instrument degassing station. Sorption at partial pressures of <0.3 provides data for BET analysis (Brunauer et al., 1938) while sorption at partial pressures of 0.3–1 provides data with which to interpret pore size distributions from gas condensation. Samples were run in both the adsorption and desorption directions over the entire partial pressure range to gain both of these types of information. Pore size distributions were calculated using the BJH method (Barrett et al., 1951), assuming slit-like geometry for the pores (Innes, 1957), as implemented on the Autosorb instrument, (see discussion in Mayer, 1994). Analyzed size ranges were from ca. 2–200 nm, representing the separation distances of opposing faces of the slits.

3. RESULTS

3.1. Microaggregate organic carbon content

The OM content of Fermilab microaggregates was four-fold lower in the cultivated, agricultural soil, compared to the native Virgin Prairie (Fig. 2, data for non-combusted samples at 20 °C and using carbon as a proxy for OM). Restoration of the cultivated soils to tallgrass prairie resulted in a doubling of the OM levels in the youngest (10-years) site, but there was little change in the OM levels over the 14 years between the youngest and oldest restored prairie sites in the chronosequence. For the Kentucky site NT resulted in the OM levels of the microaggregates (Fig. 2, 20 °C data). Higher levels of nitrogen fertilizer application led to a very small increase in OM level for the CT treatments, but a larger increase in the NT treatments.

The microaggregate samples were combusted over a range of temperatures to evaluate differences in the thermostability of the OM between treatments as an indicator of differences in the chemical composition and perhaps biochemical recalcitrance of the OM among the treatments. The loss of OM mass with temperature was greater for the microaggregates with higher initial OM levels, but the percentage decrease in OM (Fig. 2, insets) were essentially identical across all treatments at both sites. This measure of OM properties shows no systematic changes among the treatments.

In this study, we used combustion at 350 °C to remove OM from pores within the microaggregates. Combustion at 350°C removed 90% of the total OM originally in the microaggregates. OM combusted at temperatures >450 °C is generally attributed to black carbon, a broad group of charcoal-like materials (Gelinas et al., 2001; Gustafsson et al., 2001). Across all field treatments, a consistent 2–4% of the OM survived treatment at 450 °C, suggesting that black carbon is a minor component of these microaggregates.

3.2. Small angle scattering curves

Representative USAXS scattering curves are presented in Fig. 1. The figure caption provides a tutorial explanation to aid in interpreting the scattering curves.

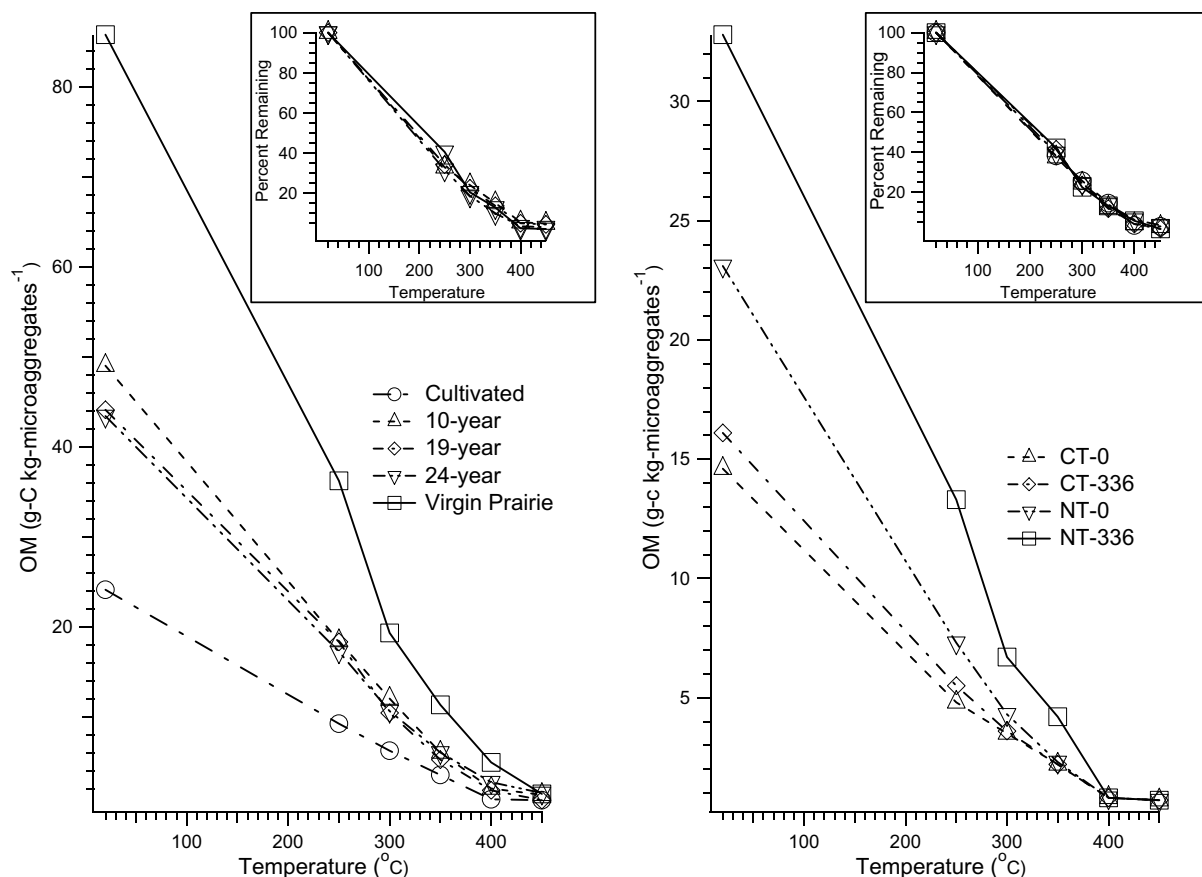


Fig. 2. Concentration of OM (expressed as $\text{g C kg microaggregates}^{-1}$) of intact microaggregates ($20\text{ }^{\circ}\text{C}$) and after combustion at $250\text{--}450\text{ }^{\circ}\text{C}$. Left panel is for Fermilab and the right panel is for Kentucky. The insets are the percent of OM remaining after combustion, compared to the OM concentration in the intact microaggregates.

It should be noted that Mayer et al. (2004) reported USAXS scattering curves from marine sediments and observed that, unlike the curves presented in Fig. 1, the combusted and intact sediment samples appeared to overlay one another, suggesting that the phenomena of OM filling voids did not occur in those sediments. Using the computational approach described here, which was not available at the time of the 2004 publication, we re-analyzed the original data for the Eel and PEM sediments presented in Mayer et al. (2004). The new analysis found that less than 1% of the sediment pore volume in the $<50\text{ nm}$ size range was occupied by OM, confirming the conclusion of that study.

3.3. Pore volume distributions by small angle scattering and N_2 sorption

The total pore volume (expressed on a mass basis ($\text{cm}^3\text{ g microaggregates}^{-1}$)) of the combusted (OM-free) microaggregates was determined by both USAXS (left panels of Figs. 3 and 4) and N_2 sorption isotherms (left panels of Fig. 5). The N_2 sorption technique has been widely applied to understanding of the pore structure of soils and sediments, and to gain insights into the distribution of OM within pores (Mayer, 1994, 1999; Bock and Mayer, 2000; Mayer and Xing, 2001; Mayer et al., 2002,

2004). However, this method is effective for a relatively narrow range of pore sizes, and can sample only the open porosity accessible to the N_2 probe molecule while X-rays penetrate the entire porosity and can evaluate porosity over a wide range of pore sizes. The configuration of our instrumentation limited us to pores $<5\text{ }\mu\text{m}$. As previously noted (Stacey, 1988; Rasmussen, 2001; Sokolowska et al., 2001), small angle scattering and N_2 sorption can yield different estimates of pore size distributions. Although the two methods assume different pore geometries (slits for the N_2 sorption approach and oblate spheroids for the USAXS approach), it is reassuring that for both the Fermilab and Kentucky microaggregates, there is very reasonable agreement (factor of 2.5 times) in the absolute values of the total pore volumes for the combusted (OM-free) samples estimated over the length scales where USAXS and N_2 sorption data overlap. Both methods yielded similar patterns of the total pore size distribution of (combusted) microaggregates from both the Fermilab and Kentucky sites. However, the N_2 sorption data yield much lower estimates of the pore volumes in the intact (uncombusted; Fig. 5 right panels), compared to combusted (OM-free) microaggregates, especially for the Fermilab samples, probably due to pore blockage of the N_2 probe molecule by OM.

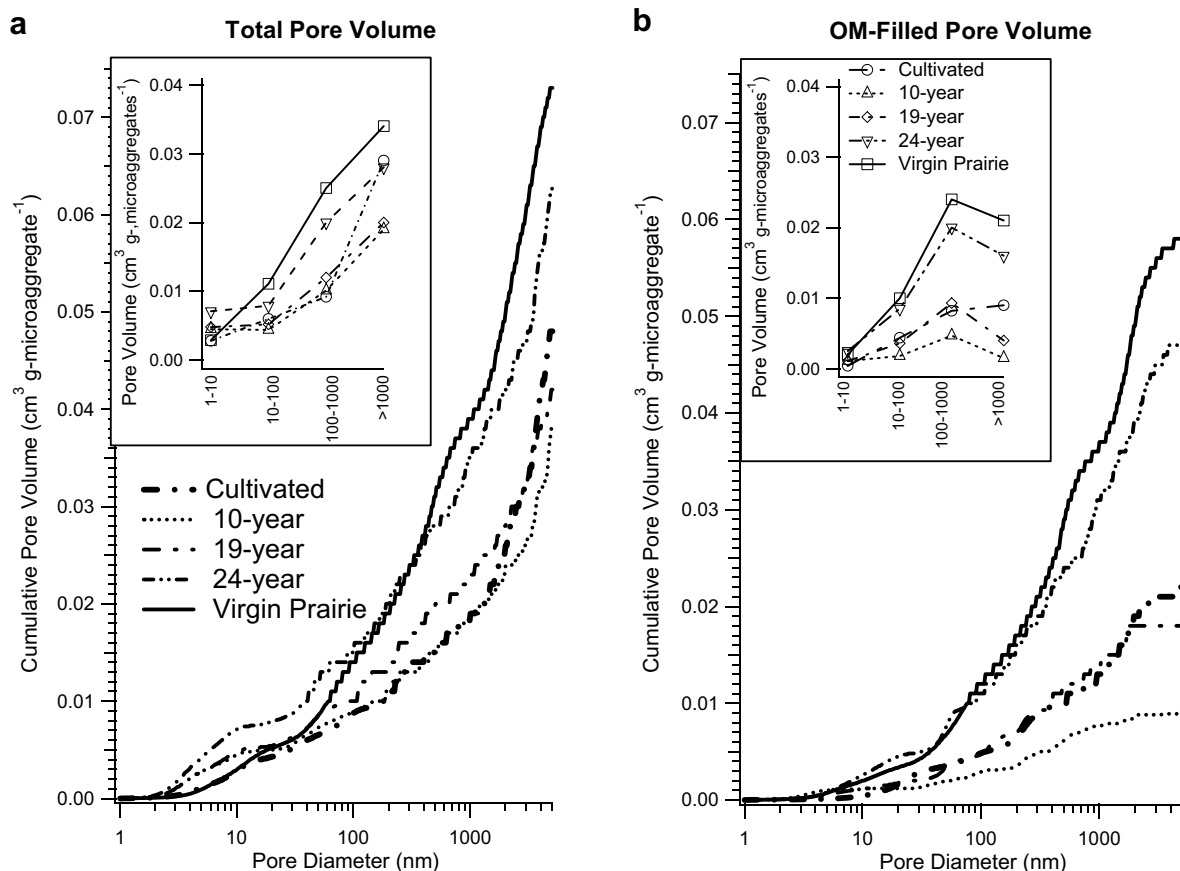


Fig. 3. Cumulative size distribution of the pore volume for microaggregates from the Fermilab experimental sites. The left panel is the size distribution of the pore volume after removal of OM by combustion at 350 °C. The right panel is the size distribution of the pore volume for the OM-filled pores. The insets are intended to assist in interpretation of the size distribution of the pore volume for different ages of prairie restoration over 4 orders-of-magnitude in pore diameters. The insets present the summed pore volumes for each sample over a smaller, decade-wide ranges of pore diameters. Each point represents the total volume within the indicated ranges of pore diameters (in nm) indicated on the abscissa.

We will focus principally on interpretation of the USAXS data because of the wider size range that can be evaluated with that method, and because the differences in the X-ray scattering length density (ρ) between minerals, OM and air provide useful information on the distribution of OM within the pores.

3.4. Total pore volume

The total pore volume of the combusted (OM-free) microaggregates determined by USAXS is presented as the main graphs of Figs. 3a and 4a. The main figures show the cumulative pore volume as a function of pore diameter. To facilitate comparisons of changes in the size distribution between treatments, the insets plot the pore volumes contained within decade-wide ranges of pore diameters.

For the Fermilab chronosequence, the magnitude and size distribution of the total pore volume differed substantially among treatments (Fig. 3a). There is perhaps a slight decrease in the total pore volume, especially for the largest pores, within 10 years of planting tallgrass prairie in the previously cultivated soil. Much later in the chronose-

quence, the pore volume increases, but it isn't until 24-years that the total pore volume approaches that of the Virgin Prairie.

The Kentucky treatments exhibit insignificant changes in the total pore volume (Fig. 4a), but lack of tillage and increased nitrogen inputs appeared to be associated with small increases in the total pore volume, especially for the largest pore diameters.

3.5. OM-filled pore volume

The size distribution of pore volume of OM-filled pores was estimated as described in Eqs. (6–9). For both the Fermilab and Kentucky sites, there are larger relative differences in the OM-filled pore volume among the different treatments, compared to the changes in the total pore volumes (Figs. 3a and 4a). For the Fermilab chronosequence, the volume of OM-filled pore initially decreased after conversion of cultivated soil to prairie, but the lost OM-filled porosity was restored between 10-year and 19-years after conversion. The pore volume distribution of the 24-year prairie is close to that of the Virgin Prairie except for the largest pore diameters.

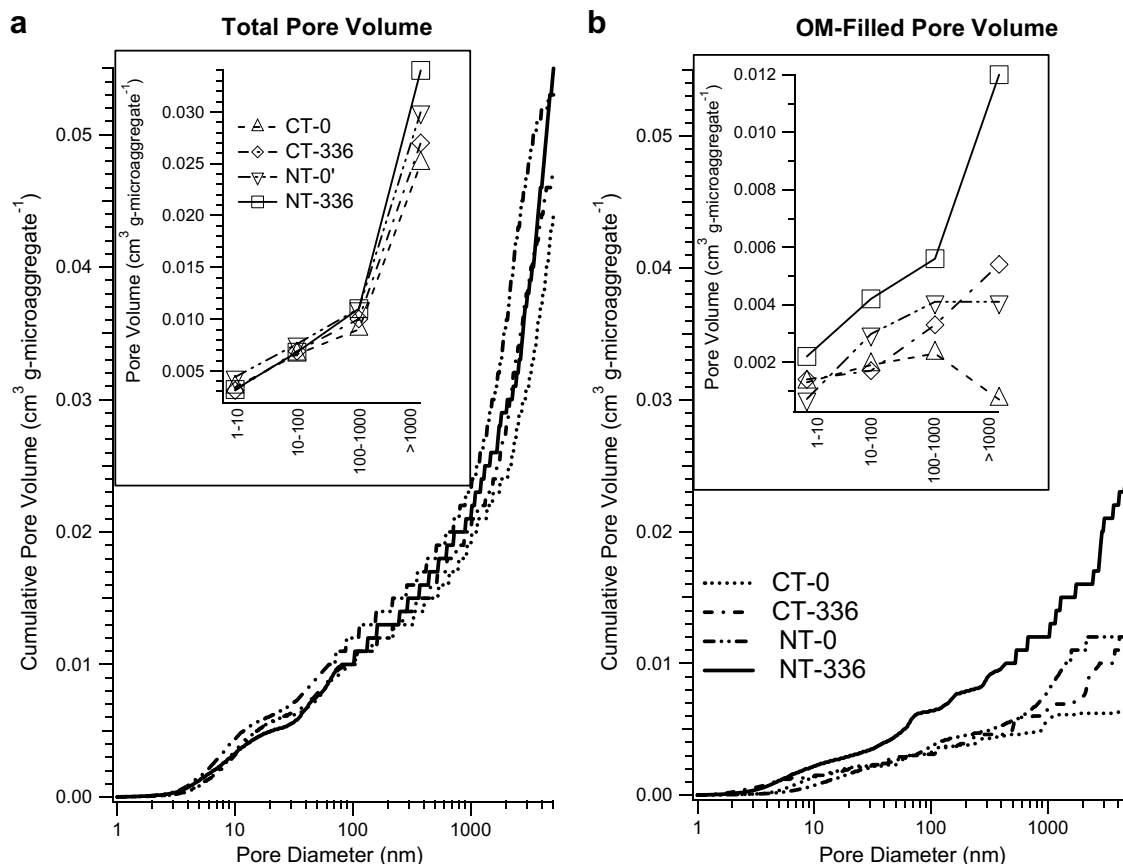


Fig. 4. Cumulative size distribution of the pore volume for the Kentucky microaggregates. The cumulative curves and insets are organized as explained in Fig. 3 for the Fermilab site.

There are large differences among treatments in the size distribution of OM-filled pores expressed as a fraction of the total porosity for each bin size and treatment (Fig. 6). Although the total pore volume is greatest in the largest pores, there is less OM-filled porosity above 1000 nm than in the 100–1000 nm size range. There is an obvious skewing of the OM distribution, with most of the pore-held OM in the 10–1000 nm size range, and smaller amounts residing in the smallest and largest pores. Conversion of cultivated soil to prairie initially results in a decrease in the relative abundance of OM-filled pores, especially in the middle size ranges. But over time, the preferential accumulation of OM in the medium-size pore classes is reestablished.

Compared to the Fermilab microaggregates, a much smaller fraction of the total porosity is filled with OM at the Kentucky site, except for the NT-336 treatment (Fig. 6). The size-dependent pattern in the OM distribution is much less strongly developed at the Kentucky site. However, for all of the Kentucky treatments, pores >1000 nm diameter had the lowest fraction of OM-filled pore volume.

3.6. Mass of OM in OM-filled pores

In addition to comparisons of pore volumes, the mass of OM in the OM-filled pores can be related to the total OM in the microaggregates, as measured with the carbon ana-

lyzer (Fig. 7). For this calculation, the volume of OM-filled pores (Figs. 3b and 4b) was converted to the mass of organic carbon in these pores (Fig. 7c and f) by assuming OM density is 1.3 g cm^{-3} and carbon constitutes 54% of the OM (Adams, 1973; Mayer et al., 2004).

For the Fermilab site, about 75% of the total mass of OM in microaggregates from the cultivated soil is located in OM-filled pores, compared with less than 60% of the Virgin Prairie microaggregates (Fig. 7b). Following prairie restoration, the total OM found in the microaggregates doubles in concentration within 10 years (Fig. 2), but the new OM is not initially located in OM-filled pores. Rather, there is a sharp decline between the cultivated and 10-year restoration in terms of the proportion of total porosity that is OM-filled, the proportion of total microaggregate-associated OM found in OM-filled pores, and the mass of OM in filled pores (Fig. 7a–c, respectively). As the prairie restoration proceeded over time, there was little change in the total microaggregate-associated OM level between 10- and 24-years (Fig. 2), but the distribution of the OM changes significantly, with OM-filled pores accounting for an increasing fraction of both the total porosity (Fig. 7a) and the total mass of OM in microaggregates (Fig. 7b). By 24-years, about 90% of the OM in the microaggregates is enclosed within OM-filled pores. Over much longer times, as represented by the Virgin Prairie, the total OM content

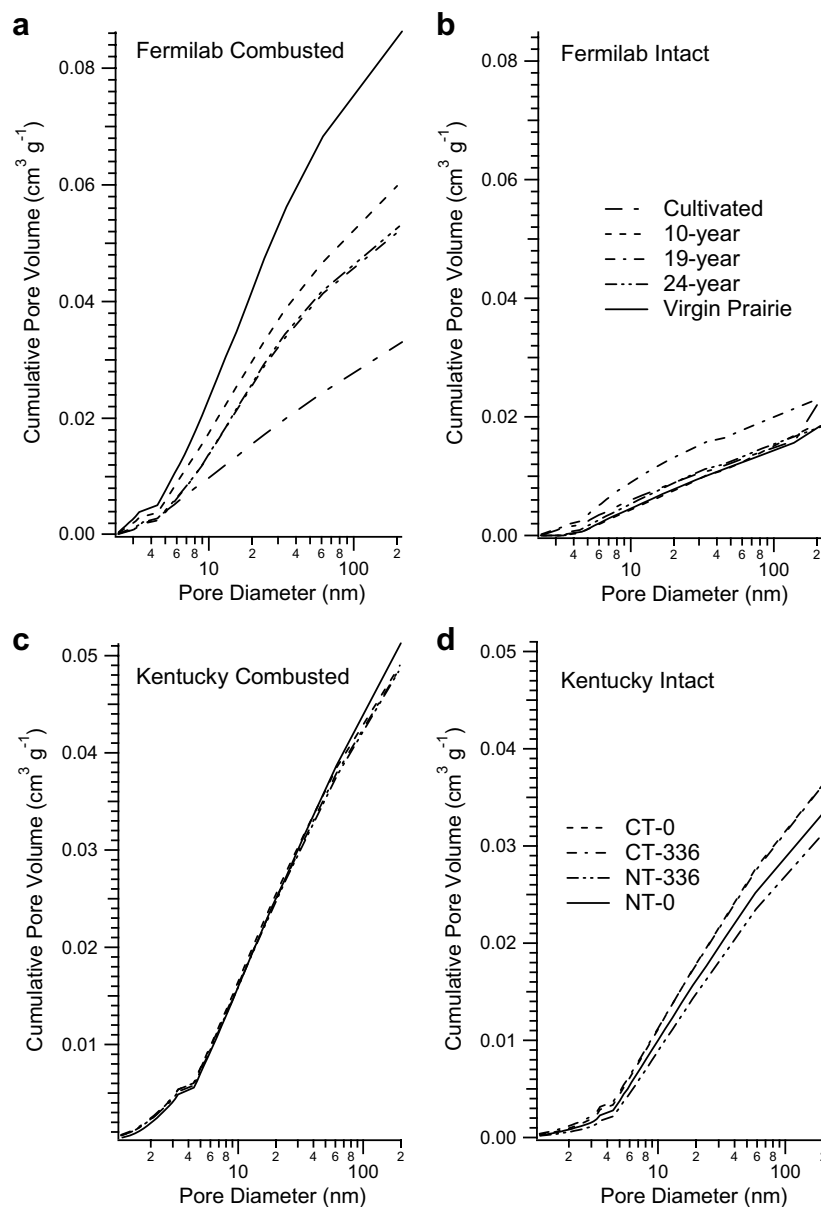


Fig. 5. The size distribution of the pore volume derived from N₂ adsorption isotherms for the Fermilab (upper panel) and Kentucky (lower panel) microaggregates. The panels on the left present the data after OM removal by combustion at 350 °C. The panels on the right are for the intact microaggregates.

of the microaggregates doubles compared to the oldest restoration (Fig. 2), but there is only a relatively small increase in the mass of OM found in filled pores (Fig. 7c). With almost 80% of the available porosity that can be accessed by the USAXS technique filled with OM (Fig. 7a), much of the additional OM in Virgin Prairie microaggregates must be located in larger pores not quantified by USAXS. Hence, the proportion of total microaggregate-associated OM found in OM-filled pores was lower in the Virgin Prairie than in the oldest restoration (Fig. 7b).

The Kentucky treatments present a straightforward pattern of OM accumulation. In treatments that result in increased OM concentrations (Fig. 2), OM-filled pores

account for an increasing fraction of the total porosity (Fig. 7d) and mass of OM (Fig. 7f), particularly for the NT-336 treatment. Nitrogen fertilization seems especially effective in promoting OM-filled porosity; for example, comparing CT-0 and CT-336, the increase of the mass of OM in filled pores (Fig. 7f) exactly matches the differences in the total mass of OM between these treatments (Fig. 2). Likewise, about two-thirds of the total OM increase resulting from fertilization of the NT treatments was localized in the OM-filled pores. In addition, nitrogen fertilization, regardless of tillage treatment, resulted in a higher proportion of microaggregate-associated OM being located within the pores accessed by USAXS (Fig. 7e).

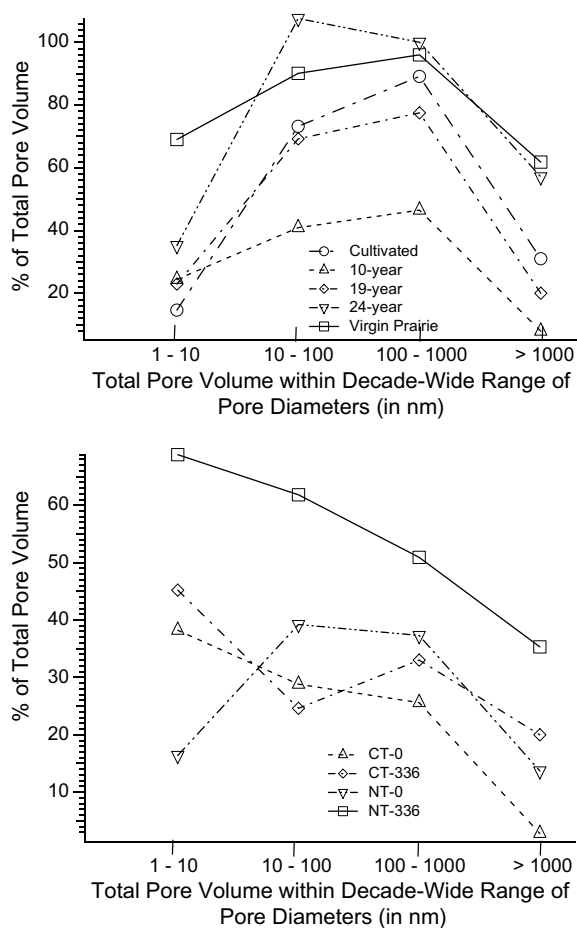


Fig. 6. The relative abundance, as a percent, of the OM-filled pore volume relative to the total pore volume within decade-wide pore diameter size classes. The upper panel is for the Fermilab chronosequence and the bottom panel is for the Kentucky site.

4. DISCUSSION

4.1. Rates of OM accumulation by microaggregates in the Fermilab chronosequence

The role of OM pore filling as a mechanism of OM accumulation in microaggregates is apparent in the comparison of the changes of the total OM and OM in submicron OM-filled pores (Table 1). There is an initial rapid increase in the total OM within microaggregates in the first 10 years following the conversion of the cultivated soil to tallgrass prairie, but thereafter, the total OM undergoes little change in the 14 years between the youngest and oldest chronosequence plots (Table 1). In the first 10 years following conversion to prairie, much of the OM accumulating inside microaggregates may be in larger particulate form, such as the organic cores described by Oades and Waters (1991) and Golchin et al. (1994). During this same period, some of the OM located within submicron pores is lost, but then OM accumulates within these pores at an accelerating pace over the remainder of the chronosequence. After 24 years in restored prairie, virtually all of the increase in total microaggregate-associated OM is accounted for by

accretion into submicron OM-filled pores. These changes can be interpreted within the context of current understanding of the evolution and turnover of soil aggregates.

4.2. Restructuring of total- and OM-filled porosity

There is a large and complex literature on the dynamics of aggregate formation and turnover (Blanco-Canqui and Lal, 2004; Six et al., 2004). The changes we observed in the total pore structure of microaggregates (i.e., combusted, OM-free) and the accumulation of OM within that evolving pore structure are consistent with models of the “lifecycles” of macro- and microaggregates. Most contemporary approaches to describing the relationship between pore structure and SOM rely on the conceptual models of Oades (1984) and Golchin et al. (1994, 1998). Golchin emphasized the role of fresh plant material in stimulating the deposition of microbially derived binding agents, causing minerals to encrust plant fragments or particulate organic matter to form very stable microaggregates. Oades (1984) revised his original hierarchy theory (Tisdall and Oades, 1982) by postulating that roots and hyphae holding together macroaggregates help to create the conditions necessary for microaggregate formation and stabilization within the macroaggregates. As these macroaggregates turnover, stable microaggregates are released and can, in turn, be incorporated into new macroaggregates (Six et al., 2000a). It is generally agreed that the architectural system of aggregate packing plays a key role in carbon sequestration (Baldoek and Skjemstad, 2000). The current study has clearly revealed a mechanism that contributes to the development of this soil architectural system and the stabilization of OM within that system. We propose that pore-filling by OM, largely in submicron pores, is an important mechanism for protecting OM within microaggregates.

Although the microaggregates from the Cultivated site at Fermilab have relatively low levels of microaggregate-associated OM compared to the prairie treatments (Fig. 2), OM filled 40% of the total submicron porosity (Fig. 7a). Further, about 75% of the total OM in Cultivated site microaggregates is retained within those protected OM-filled pores (Fig. 7b), suggesting that OM filling in pores provides a protected refuge for OM in the Cultivated microaggregates.

The OM content of the microaggregates rapidly increased after conversion to tallgrass prairie; after 10 years the OM content was more than twice that of the original cultivated field (Fig. 2). However, none of this initial increase in OM appears to be associated with OM-filled pores. In microaggregates from the 10-year prairie, OM-filled pores accounted for less than 20% of the total porosity (Fig. 7a) and about 10% of the total OM in the microaggregates (Fig. 7b). The extensive system of roots and mycorrhizal hyphae in tallgrass prairie promotes rapid restoration of aggregate structure. At the Fermilab site the abundance of macroaggregates increased from approximately 40% of the total soil in the cultivated plots to over 90% of the soil within 10 years of planting to tallgrass prairie (Jastrow, 1987, 1996; Jastrow et al., 1998). Given the prevailing model that microaggregates develop within macroaggregates, the feed-

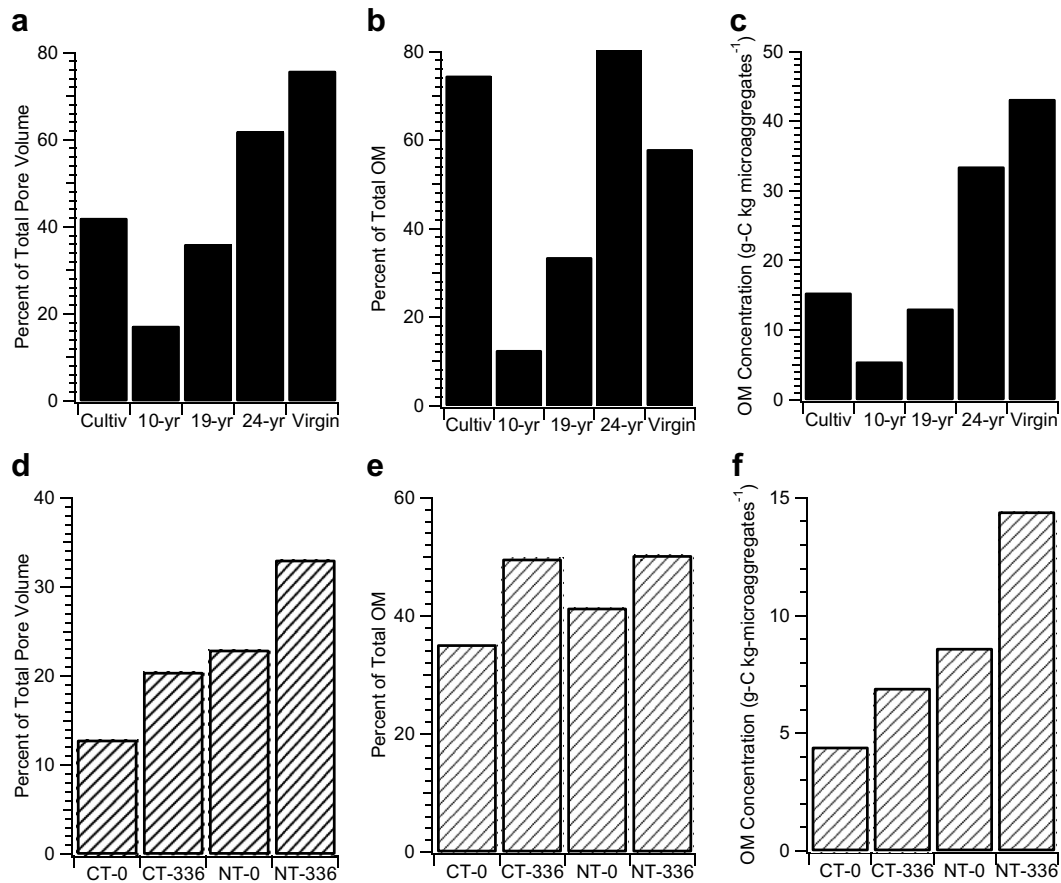


Fig. 7. Distribution of OM within microaggregates. Top panels (a–c) are for the Fermilab chronosequence and the bottom panels (d–f) are for Kentucky site; (a and d) are the percentage of measured microaggregate pore volume that is OM-filled; (b and e) are the percentage of the total mass of microaggregate-associated OM located in OM-filled pores; (c and f) are the concentration of OM (measured as organic carbon) found in OM-filled pores of microaggregates.

Table 1

Annualized rate of total OM accumulation (calculated from data for 20 °C in Fig. 2a) compared to the annualized rate of OM accumulation within OM-filled pores (calculated from the total cumulative mass of OM in Fig. 3b) of microaggregates during 24 years of tallgrass prairie restoration in the Fermilab chronosequence

Time interval (years)	Accumulation of total OM ^a in microaggregates (g C kg microaggregates ⁻¹ yr ⁻¹)	Accumulation of OM in OM-filled pores (g C kg microaggregates ⁻¹ yr ⁻¹)
0–10	2.7	–0.11
10–19	–0.5	0.84
18–24	–0.1	3.4
0–24	0.8	0.75

^a OM is expressed as the organic carbon content of intact microaggregates (20 °C) (Fig. 2).

back processes of OM deposition and microaggregate stabilization lag behind the developing macroaggregate structure. The high SFA of the 10-yr treatment (Table 2)

suggests that during the first 10 years of the chronosequence there is a much higher percentage of unaggregated small clay mineral particles available to associate with new OM, and also participate in the early phases of aggregate development by encrusting OM deposited during the first 10 years of the chronosequence. With the microaggregate “incubator” fully operational after the 10th growing season, there is a progressive increase in the fraction of the total porosity that is OM-filled, and submicron OM-filled pores constitute an increasing proportion of the OM in the 19- and 24-year samples (Fig. 7a–c).

The design of the Kentucky experiment makes it more difficult to evaluate the evolution of microaggregate pore structure and pore filling, but there are striking contrasts between the extent, and possibly the importance, of pore-filling in protecting OM in the Fermilab and Kentucky systems. The contrast between sites likely reflects differences in the soil type and the nature of the interactions that stabilize the structure of the microaggregates. In Mollisols and other soils dominated by 2:1 clay minerals, OM is the principal agent stabilizing the aggregate structure (Oades and Waters, 1991; Six et al., 2000b). The pattern we observed in the restructuring of the porosity at Fermilab is consistent

Table 2

The specific surface area (SFA) of combusted microaggregates, measured by N₂ adsorption, and the ratio of the total microaggregate organic carbon content (Fig. 2, 20 °C) relative to the SFA (OC:SFA)

Fermilab	Cultivated	10-year	19-year	24-year	Virgin Prairie
SFA (m ² g ⁻¹)	15.30	32.65	27.95	26.95	39.35
OC:SFA (mg C m ⁻²)	1.6	1.5	1.6	1.6	2.2
Kentucky	CT-0	CT-336	NT-0	NT-336	
SFA (m ² g ⁻¹)	27.3	26.9	25.9	24.2	
OC:SFA (mg C m ⁻²)	0.5	0.6	0.9	1.4	

with the importance of OM in development and maintenance of microaggregate structure in Mollisols.

In soils characterized by 1:1 clays and oxides, such as those of the Kentucky site (Six et al., 2000b), electrostatic attractions between mineral surfaces are more dominant stabilizing agents, and aggregate hierarchy is not as strong or absent (Oades and Waters, 1991; Muggler et al., 1999). The abundance of oxides in the Kentucky soils (Karathanasis, 1991) is consistent with our observations that, across the combination of tillage and nutrient treatments of the microaggregates, there is little, if any, difference in the total porosity (Fig. 4a). However, there is significant restructuring of the OM-filled porosity (Fig. 4b), likely by mechanisms similar to those described for the Fermilab microaggregates. Six et al. (2000b) documented a higher abundance of carbon in both macro- and microaggregates in the Kentucky NT, compared to CT plots. The absence of tillage and increased nitrogen inputs result in significant increases in the relative abundance of OM-filled pores (Fig. 7d), the fraction of the total microaggregate-associated OM enclosed in OM-filled pores (Fig. 7e), and the mass of OM in submicron OM-filled pores (Fig. 7f). The absence of tillage combined with added nitrogen inputs had the greatest impact on both OM accrual and OM-filled porosity.

4.3. Mechanisms for protection of OM

Our results allow some assessment of whether sequestration of OM within microaggregates protects organic matter via organic recalcitrance or biotic exclusion.

1. *Biochemical stabilization:* The thermal stability of microaggregate-associated OM was determined as an indicator of compositional differences in OM that reflect changes in the chemical recalcitrance of the OM. For example, Grisi et al. (1998) compared OM from tropical and temperate soils with respect to microbial biomass, OM decomposition rates, and thermogravimetric and differential thermal analyses. OM was mineralized much more rapidly in the temperate than tropical soils, indicating that the OM from the tropical soil was more degraded. Thermal analyses indicated that the tropical soils were also less thermally labile than the temperate soil. Similar conclusions were reported for the isolated humic acid fractions of the same soils. Likewise, pyrolysis-field ionization mass spectroscopy has demonstrated differences in the thermal lability of more biologically

labile, compared to less-readily metabolized OM (Kalbitz et al., 2003), as well as between OM in heavy density fractions of soil compared to the light fractions composed of fresher plant-derived material (Schulten and Leinweber, 1999). The microaggregate-associated OM in this study showed no change in the thermal lability with either prairie restoration or tillage/fertilization treatments (Fig. 2, insets), suggesting that the differences in OM accumulation were not related to compositional changes that might result in biochemical protection of the OM. Further chemical characterization of the nature of the OM in filled pores is needed to verify this inference.

2. *Biotic exclusion by aggregate structures:* We propose that a significant mechanism for OM preservation in many soils results from the architectural packing system emerging during microaggregate formation (Oades, 1984; Golchin et al., 1994, 1998) which encloses, or encapsulates, colloid-sized particles of OM with minerals, creating pores that are filled with OM. The minerals have been suggested to serve as a physical barrier in protection of OM from degradation in pores too small to permit access to the OM by microbes, enzymes or oxidants (Baldock and Skjemstad, 2000).

We confirm here the conclusions of Mayer and coworkers (Mayer, 1994; Mayer et al., 2004) that OM is not protected in small mesopores (2–10 nm) that are small enough to exclude exoenzymes that degrade OM (3–4 nm) (Zimmerman et al., 2004). Instead, most of the OM resides in pore size ranges that could accommodate exoenzymes and even small bacteria (Figs. 3, 4, and 6). There is, however, generally a sharp drop in the fraction of OM-filled porosity in pores with >1 μm pore diameters (Fig. 6), which is consistent with the selective loss of OM in pores that could enclose a large bacterium, potentially in direct contact with OM. Nevertheless, a sufficient pore size to hold exoenzymes does not mean that enzymes from organisms outside the pore have full access to the OM held within.

Extracellular enzymes are the primary means by which soil microbes degrade complex organic materials into assimilable small molecules. OM decomposition is not, as usually described, a simple first order process with respect to OM concentration, but is also first order with respect to the concentration of exoenzymes reacting with the OM (Schimel and Weintraub, 2003). If, on microbial time scales, the OM pool can be considered large (not limiting) and relatively unchanging, decomposition kinetics become zero-

order on OM concentration. Under these conditions, microbial growth and OM degradation are dictated by the kinetics of enzyme production and by the diffusion of enzyme to OM and hydrolysate back to the microorganism (Vetter et al., 1998). The key to OM preservation derives from the economic rules of “return on investment” microbes get for producing exoenzymes. Any process that limits the access of the enzymes to the OM reduces net energy gain, possibly leading to microbial starvation (Schimel and Weintraub, 2003).

Mineral encapsulation could protect against hydrolysis in several ways. First, it limits enzyme access to the small “throats” of OM-filled pores (Mayer et al., 2004), protecting the bulk of the OM within the pore body. The lower pore volumes measured by gas adsorption for intact microaggregates (Fig. 5), compared to the combusted, OM-free samples, may be due to blocking of pore throats by OM, thus preventing access of the N₂ probe molecule into the pore space. If OM excludes a N₂ molecule (cross sectional area of 1.6 nm), then even small (3–4 nm) exoenzymes would be excluded from filled pores and would have access only via the pore throat. Thus, only a small fraction of the OM in filled pores (Fig. 7c and f) is accessible for enzymatic hydrolysis. Although microbial enzymes and hydrolysis products might follow pathways through pores that were not filled with OM to reach more distant pools of OM, a network of OM-filled pores could increase the tortuosity of such pathways and thereby reduce the rate of delivery of assimilable nutrients to the microbes. Both effective reduction in the accessible OM pool and kinetic constraints on the abundance and connectivity of pores available for diffusion could make it energetically unfavorable for continued microbial enzyme production, growth or even survival (Simoni et al., 2001; Allison, 2005; Allison and Vitousek, 2005; Ekschmitt et al., 2005).

5. SUMMARY AND CONCLUSIONS

This study sought to understand the mechanisms by which OM is preserved in soil microaggregates by investigating the internal pore structure of microaggregates and the distribution of OM within those pores. Changes in land use or agricultural management affect the degree of soil disturbance as well as the nature and amount of organic inputs and the root structure of the soil. These changes affect the formation and turnover of macro- and microaggregates. Our results suggest that the key process in the protection of OM in soil microaggregates is related to the architectural system of aggregate packing. Our novel application of USAXS revealed aspects of that architectural packing and demonstrated that OM preservation is the result of new inputs of OM becoming encapsulated by minerals, probably during microaggregate formation and turnover. We postulate that the protection arises from spatial and kinetic constraints imposed on the ability of microbial exoenzymes to access and degrade the OM and on the delivery of hydrolysis products that can be assimilated by the microbes. Simple economic rules of “return on investment” suggest that this protection mechanism may have long-term impacts on microbial growth and even survival.

5.1. Environmental implications: sequestration capacity and feedbacks

The recognition of pore-filling as a protective mechanism has important consequences in predictions of carbon-sequestration potential of soil and in evaluating strategies to enhance sequestration.

1. *Limitation on the capacity to stabilize OM in soil:* The preservation of OM by its association with minerals has been the focus of many studies. Recently, however, the importance of sorptive preservation has been questioned because of the limited sorptive capacity of minerals (Six et al., 2002; Guggenberger and Kaiser, 2003). Mineral encapsulation may provide greater potential for OM preservation before saturation of the mechanism because a greater volume of OM can be enclosed within a given surface area of minerals than can be adsorbed onto surfaces. Furthermore, we have demonstrated that the extent of preservation of OM by the pore-filling mechanism can be affected by agricultural management or land use, suggesting the possibility of strategies to ameliorate global climate change through agricultural management alternatives.
2. *Feedback loops:* The progression of OM accrual and the extent of pore-filling over time suggest that the magnitude of OM accrual and preservation can be enhanced dramatically if effective management alternatives are sustained over time. Further, application of such strategies may also increase the extent of OM preservation in soil. Conversely, practices that perturb the pore structure of soil and destroy the architectural system of OM-filled porosity, or accelerate the dynamics of aggregate formation and turnover are likely to result in significant losses of soil OM that may take a long time to reverse.

This study has developed a new tool (USAXS) to obtain critical information on the mechanisms of OM protection in soil aggregates. Using this tool, we have demonstrated its effectiveness in evaluating strategies to enhance carbon-sequestration in soil through changes in agricultural management practices and land use. This approach could be applied across a much wider range of sites to evaluate the general importance of the pore-filling protection mechanism along gradients of soil types, vegetation, and climate.

ACKNOWLEDGMENTS

This research was supported by the National Science Foundation (EAR-0223279), the U.S. Department of Agriculture's National Research Initiative (2002-35107-12677), the Petroleum Research Fund (39880-AC28 and 38466-AC2), and the U.S. Department of Energy (DOE), Office of Science, Office of Biological and Environmental Research, Climate Change Research Division under contract DE-AC02-06CH11357.

The Ultra-Small Angle Scattering (USAXS) data were obtained at the UNICAT facility of the Advanced Photon Source (APS) at Argonne National Laboratory. The UNICAT facility is supported by the U.S. DOE under Award No. DEFG02-91ER45439, through the Frederick Seitz Materials Research Laboratory at the University of Illinois at Urbana-Champaign and the Oak Ridge National

Laboratory (U.S. DOE contract DE-AC05-00OR22725 with UT-Battelle LLC). Interpretation of the USAXS data was assisted by the National Institute of Standards and Technology (U.S. Department of Commerce) and UOP LLC. The APS is supported by the U.S. DOE, Office of Science, Office of Basic Energy Sciences under contract DE-AC02-06CH11357. We thank S. O'Brien and K. Moran for isolating the microaggregates. We also acknowledge and thank the associate editor and two anonymous reviewers who identified very critical issues that were invaluable in helping us to greatly improve this manuscript.

REFERENCES

- Adams W. A. (1973) The effect of organic matter on the bulk and true densities of some uncultivated podzolic soils. *J. Soil. Sci.* **24**, 10–17.
- Allison S. D. (2005) Cheaters, diffusion and nutrients constrain decomposition by microbial enzymes in spatially structured environments. *Ecol. Lett.* **8**, 626–635.
- Allison S. D. and Vitousek P. M. (2005) Responses of extracellular enzymes to simple and complex nutrient inputs. *Soil Biol. Biochem.* **37**, 937–944.
- Allison V. J., Miller R. M., Jastrow J. D., Matamala R. and Zak D. R. (2005) Changes in soil microbial community structure in a tallgrass prairie chronosequence. *Soil. Sci. Soc. Am. J.* **69**, 1412–1421.
- Angers D. A., Recous S. and Aita C. (1997) Fate of carbon and nitrogen in water-stable aggregates during decomposition of $^{13}\text{C}^{15}\text{N}$ -labeled wheat straw in situ. *Eur. J. Soil Sci.* **48**, 1412–1421.
- Antxustegi M. M., Hall P. J. and Calo J. M. (1998a) Development of porosity in Pittsburgh No. 8 coal char as investigated by contrast-matching small-angle neutron scattering and gas adsorption techniques. *Energ. Fuel* **12**, 542–546.
- Antxustegi M. M., Hall P. J. and Calo J. M. (1998b) The use of contrast-matching small-angle neutron-scattering techniques to monitor closed porosity in carbons. *J. Colloid Interface Sci.* **202**, 490–498.
- Avdeev M. V. (2007) Contrast variation in small-angle scattering experiments on polydisperse and superparamagnetic systems: basic functions approach. *J. Appl. Crystallogr.* **40**, 56–70.
- Baldock J. A. and Skjemstad J. O. (2000) Role of the soil matrix and minerals in protecting natural organic materials against biological attack. *Org. Geochem.* **31**, 697–710.
- Balesdent J., Chenu C. and Balabane M. (2000) Relationship of soil organic matter dynamics to physical protection and tillage. *Soil Tillage Res.* **53**, 215–230.
- Barrett E. G., Joyner L. G. and Halenda P. P. (1951) The determination of pore volume and area distributions in porous substances. I. Computations from nitrogen isotherms. *J. Am. Chem. Soc.* **73**, 373–380.
- Bartlett R. and James B. (1980) Studying dried, stored soil samples — Some pitfalls. *Soil Sci. Soc. Am. J.* **44**, 721–724.
- Besnard E., Chenu C., Balesdent J., Puget P. and Arrouays D. (1996) Fate of particulate organic matter in soil aggregates during cultivation. *Eur. J. Soil Sci.* **47**, 495–503.
- Bihannic I., Tchoubar D., Lyonard S., Besson G. and Thomas F. (2001) X-ray scattering investigation of swelling clay fabric 1. The dry state. *J. Colloid Interface Sci.* **240**, 211–218.
- Blanco-Canqui H. and Lal R. (2004) Mechanisms of carbon sequestration in soil aggregates. *Crit. Rev. Plant Sci.* **23**, 481–504.
- Bock M. J. and Mayer L. M. (2000) Mesodensity organo-clay associations in a near-shore sediment. *Mar. Geol.* **163**, 65–75.
- Borkovec M., Wu Q., Degovics G., Laggner P. and Sticher H. (1993) Surface-area and size distributions of soil particles. *Colloids Surf. A Physicochem. Eng. Aspects*, 65–76.
- Bossuyt H., Six J. and Hendrix P. F. (2002) Aggregate-protected carbon in no-tillage and conventional tillage agroecosystems using carbon-14 labeled plant residue. *Soil. Sci. Soc. Am. J.* **66**, 1965–1973.
- Brunauer S., Emmett P. H. and Teller E. (1938) Adsorption of gases in multimolecular layers. *J. Am. Chem. Soc.* **60**, 309–319.
- Calo J. M., Hall P. J. and Antxustegi M. (2001) Carbon porosity characterization via small angle scattering. *Colloids Surf. A Physicochem. Eng. Aspects* **187–188**, 219–232.
- Campbell C. A. (1978) Soil organic carbon, nitrogen and fertility. In *Soil Organic Matter*, vol. 8 (eds. M. Schnitzer and S. U. Khan), pp. 173–271. Developments in Soil Science. Elsevier Scientific, Amsterdam.
- Carrado K. A. and Xu L. Q. (1999) Materials with controlled mesoporosity derived from synthetic polyvinylpyrrolidone-clay composites. *Micropor. Mesopor. Mat.* **27**, 87–94.
- Carrado K. A., Csencsits R., Thiagarajan P., Seifert S., Macha S. M. and Harwood J. S. (2002) Crystallization and textural porosity of synthetic clay minerals. *J. Mater. Chem.* **12**, 3228–3237.
- Christensen B. T. (2001) Physical fractionation of soil and structural and functional complexity in organic matter turnover. *Eur. J. Soil Sci.* **52**, 345–353.
- Conen F., Leifeld J., Seth B. and Alewell C. (2006) Warming mineralises young and old soil carbon equally. *Biogeosciences* **3**, 515–519.
- Dalal R. C. and Bridge B. J. (1996) Aggregation and organic matter storage in sub-humid and semi-arid soils. In *Structure and Organic Matter Storage in Agricultural Soils* (eds. M. R. Carter and B. A. Stewart). CRC Press, pp. 263–307.
- Denef K., Six J., Paustian K. and Merckx R. (2001) Importance of macroaggregate dynamics in controlling soil carbon stabilization: short-term effects of physical disturbance induced by dry-wet cycles. *Soil Biol. Biochem.* **33**, 2145–2153.
- Dexter A. R. (1988) Advances in characterization of soil structure. *Soil Tillage Res.* **11**, 199–238.
- Diallo M. S., Glinka C. J., Goddard W. A. and Johnson J. H. (2005) Characterization of nanoparticles and colloids in aquatic systems 1. Small angle neutron scattering investigations of Suwannee river fulvic acid aggregates in aqueous solutions. *J. Nanoparticle Res.* **7**, 435–448.
- Ekschmitt K., Liu M. Q., Vetter S., Fox O. and Wolters V. (2005) Strategies used by soil biota to overcome soil organic matter stability—why is dead organic matter left over in the soil? *Geoderma* **128**, 167–176.
- Elliott E. T. and Coleman D. C. (1988) Let the soil work for us. *Ecol. Bull.* **39**, 23–32.
- Feller C. and Beare M. H. (1997) Physical control of soil organic matter dynamics in the tropics. *Geoderma* **79**, 69–116.
- Frye W. W. and Blevins R. L. (1997) Soil organic matter under long-term no-tillage and conventional tillage corn production in Kentucky. In *Soil Organic Matter in Temperate Agroecosystems* (eds. E. A. Paul, K. Paustian, E. T. Elliott and C. V. Cole). CRC Press, Boca Raton, pp. 227–234.
- Gale W. J., Cambardella C. A. and Bailey T. B. (2000) Root-derived carbon and the formation and stabilization of aggregates. *Soil Sci. Soc. Am. J.* **64**, 201–207.
- Gelinas Y., Prentice K. M., Baldock J. A. and Hedges J. I. (2001) An improved thermal oxidation method for the quantification of soot/graphitic black carbon in sediments and soils. *Environ. Sci. Technol.* **35**, 3519–3525.
- Glatter O. and Kratky O. (1982) *Small-Angle X-ray Scattering*. Academic Press, New York.

- Golchin A., Oades J. M., Skjemstad J. O. and Clarke P. (1994) Soil-structure and carbon cycling. *Aust. J. Soil Res.* **32**, 1043–1068.
- Golchin A., Baldock J. A. and Oades J. M. (1998) A model linking organic matter decomposition, chemistry and aggregate dynamics. In *Soil Processes and the Carbon Cycle* (eds. R. Lal, J. M. Kimble, R. F. Follett and B. A. Stewart). CRC Press, Boca Raton, pp. 245–266.
- Gregorich E. G., Kachanoski R. G. and Voroney R. P. (1989) Carbon mineralization in soil size fractions after various amounts of aggregate disruption. *J. Soil Sci.* **40**, 649–659.
- Grisi B., Grace C., Brookes P. C., Benedetti A. and Dell'Abate M. T. (1998) Temperature effects on organic matter and microbial biomass dynamics in temperate and tropical soils. *Soil Biol. Biochem.* **30**, 1309–1315.
- Guggenberger G. and Kaiser K. (2003) Dissolved organic matter in soil: challenging the paradigm of sorptive preservation. *Geoderma* **113**, 293–310.
- Guinier A. a. and Fournet G. (1955) *Small-Angle Scattering of X-rays*. John Wiley and Sons, Inc., New York.
- Gustafsson O., Bucheli T. D., Kukulska Z., Andersson M., Largeau C., Rouzaud J. N., Reddy C. M. and Eglinton T. I. (2001) Evaluation of a protocol for the quantification of black carbon in sediments. *Global Biogeochem. Cycles* **15**, 881–890.
- Hall P. J., Galan D. G., Machado W. R., Mondragon F., Barria E. B., Sherrington D. C. and Calo J. M. (1997) Use of contrast-enhanced small-angle neutron scattering to monitor the effects of solvent swelling on the pore structure of styrene-divinylbenzene resins. *J. Chem. Soc. Faraday Trans.* **93**, 463–466.
- Innes W. B. (1957) Use of a parallel plate model in calculation of pore size distribution. *Anal. Chem.* **29**, 1069–1073.
- Jastrow J. D. (1987) Changes in soil aggregation associated with tallgrass prairie restoration. *Am. J. Bot.* **74**, 1656–1664.
- Jastrow J. D. (1996) Soil aggregate formation and the accrual of particulate and mineral-associated organic matter. *Soil Biol. Biochem.* **28**, 665–676.
- Jastrow J. D. and Miller R. M. (1998) Soil aggregate stabilization and carbon sequestration: feedbacks through organomineral associations. In *Soil Processes and the Carbon Cycle* (eds. R. Lal, J. M. Kimble, R. F. Follett and B. A. Stewart). CRC Press, pp. 207–228.
- Jastrow J. D., Miller R. M. and Lussenhop J. (1998) Contributions of interacting biological mechanisms to soil aggregate stabilization in restored prairie. *Soil Biol. Biochem.* **30**, 905–916.
- Jemian P. R., Weertman J. R., Long G. G. and Spal R. D. (1991) Characterization of 9Cr-1MoVNb steel by anomalous small-angle X-ray scattering. *Acta Metall. Mater.* **39**, 2477–2487.
- Kalbitz K., Schwesig D., Schmerwitz J., Kaiser K., Haumaier L., Glaser B., Ellerbrock R. and Leinweber P. (2003) Changes in properties of soil-derived dissolved organic matter induced by biodegradation. *Soil Biol. Biochem.* **35**, 1129–1142.
- Karathanasis A. D. (1991) Phosphate mineralogy and equilibria in 2 Kentucky Alfisols derived from ordovician limestones. *Soil Sci. Soc. Am. J.* **55**, 1774–1782.
- Kemper W. D. and Rosenau R. C. (1984) Soil cohesion as affected by time and water content. *Soil Sci. A. J.* **48**, 1001–1006.
- Kilbertus G. (1980) Study of microhabitats in soil aggregates—relation to bacterial biomass and size of prokaryotes. *Rev. D Ecol. Biol. Du Sol* **17**, 543–557.
- Kirby N., Cookson D., Buckley C., Bovell E. and St Pierre T. (2007) Iron K-edge anomalous small-angle X-ray scattering at 15-D-D at the advanced photon source. *J. Appl. Crystallogr.* **40**, S402–S407.
- Klitzke S. and Lang F. (2007) Hydrophobicity of soil colloids and heavy metal mobilization: effects of drying. *J. Environ. Qual.* **36**, 1187–1193.
- Kotzias D., Herrmann M., Zsolnay A., Beyerle-Pfnur R., Parlar H. and Korte F. (1987) Photochemical aging of humic substances. *Chemosphere* **16**, 1463–1468.
- Lee B., Lo C. T., Seifert S., Rago N. L. D., Winans R. E. and Thiyagarajan P. (2007) Anomalous small-angle X-ray scattering characterization of bulk block copolymer/nanoparticle composites. *Macromolecules* **40**, 4235–4243.
- Long G. G., Allen A. J., Ilavsky J., Jemian P. R. and Zschack P. (2000) The ultra-small-angle X-ray scattering instrument on UNICAT at the APS. In *11th U.S. National Synchrotron Radiation Instrumentation Conference (SRI99)*, vol. 521 (eds. P. Pianetta and H. Winick). American Institute of Physics, New York, pp. 183–187.
- Mayer L. M. (1994) Surface-area control of organic-carbon accumulation in continental-shelf sediments. *Geochim. Cosmochim. Acta* **58**, 1271–1284.
- Mayer L. M. (1999) Extent of coverage of mineral surfaces by organic matter in marine sediments. *Geochim. Cosmochim. Acta* **63**, 207–215.
- Mayer L. M. (2004) The inertness of being organic. *Mar. Chem.* **92**, 135–140.
- Mayer L. M. and Xing B. S. (2001) Organic matter–surface area relationships in acid soils. *Soil Sci. Soc. Am. J.* **65**, 250–258.
- Mayer L. M., Benninger L., Bock M., DeMaster D., Roberts Q. and Martens C. (2002) Mineral associations and nutritional quality of organic matter in shelf and upper slope sediments off Cape Hatteras, USA: a case of unusually high loadings. *Deep-Sea Res. II Top. Stud. Oceanogr.* **49**, 4587–4597.
- Mayer L. M., Schick L. L., Hardy K. H., Wagai R. and McCarthy J. F. (2004) Organic matter in small mesopores in sediments and soil. *Geochim. Cosmochim. Acta* **68**, 3863–3872.
- Muggler C. C., Griethuysen C. v., Buurman P. and Pape T. (1999) Aggregation, organic matter, and iron oxide morphology in oxisols from Minas Gerais, Brazil. *Soil Sci.* **164**, 759–770.
- Oades J. M. (1984) Soil organic-matter and structural stability—mechanisms and implications for management. *Plant Soil* **76**, 319–337.
- Oades J. M. and Waters A. G. (1991) Aggregate hierarchy in soils. *Aust. J. Soil Res.* **29**, 815–828.
- Peltovuori T. and Soenne H. (2005) Phosphorus solubility and sorption in frozen, air-dried and field-moist soil. *Eur. J. Soil Sci.* **56**, 821–826.
- Post W. M., Izaurrealde R. C., Jastrow J. D., McCarl B. A., Amonette J. E., Bailey V. L., Jardine P. M., West T. O. and Zhou J. Z. (2004) Enhancement of carbon sequestration in US soils. *Bioscience* **54**, 895–908.
- Potton J. A., Daniell G. J. and Rainford B. D. (1986) Application of maximum entropy to small-angle neutron scattering data and liquid and amorphous material diffraction data analysis. *Inst. Phys. Conf. Ser. #81*, 61–86, Chapter 3.
- Potton J. A., Daniell G. J. and Rainford B. D. (1988) Particle size distributions from SANS data using the maximum entropy method. *J. Appl. Crystallogr.* **21**, 663–668.
- Pranzas P. K., Dornheim M., Bosenberg U., Fernandez J. R. A., Goerigk G., Roth S. V., Gehrke R. and Schreyer A. (2007) Small-angle scattering investigations of magnesium hydride used as a hydrogen storage material. *J. Appl. Crystallogr.* **40**, S402–S407.
- Radlinski A. P. and Hinde A. L. (2001) Applications of small angle neutron and small angle X-ray scattering to petroleum geology. In *Environmental Studies Using Neutron and Synchrotron Facilities*. ILL/ESRF, Grenoble, 20–21 February 2001.
- Radlinski A. P., Mastalerz M., Hinde A. L., Hainbuchner M., Rauch H., Baron M., Lin J. S., Fan L. and Thiyagarajan P. (2004) Application of SAXS and SANS in evaluation of

- porosity, pore size distribution and surface area of coal. *Int. J. Coal Geol.* **59**, 245–271.
- Rasmussen F. B. (2001) Different approaches to analysis of small angle scattering experiments on porous aluminum hydroxide. *Colloid Surf. A Physicochem. Eng. Aspects* **187–188**, 327–335.
- Rice J. A., Tombacz E. and Malekani K. (1999) Applications of light and X-ray scattering to characterize the fractal properties of soil organic matter. *Geoderma* **88**, 251–264.
- Sahoo P. K., Soltani S., Wong A. K. C. and Chen Y. C. (1988) A survey of thresholding techniques. *Comput. Vision Graph. Image Process.* **41**, 233–260.
- Sastry P. U., Sen D., Mazumder S. and Chandrasekaran K. S. (2000) Structural variations in lignite coal: a small angle X-ray scattering investigation. *Solid State Commun.* **114**, 329–333.
- Schimel J. P. and Weintraub M. N. (2003) The implications of exoenzyme activity on microbial carbon and nitrogen limitation in soil: a theoretical model. *Soil Biol. Biochem.* **35**, 549–563.
- Schulten H. R. and Leinweber P. (1999) Thermal stability and composition of mineral-bound organic matter in density fractions of soil. *Eur. J. Soil Sci.* **50**, 237–248.
- Simoni S. F., Schafer A., Harms H. and Zehnder A. J. B. (2001) Factors affecting mass transfer limited biodegradation in saturated porous media. *J. Contam. Hydrol.* **50**, 99–120.
- Six J., Elliott E. T. and Paustian K. (2000a) Soil macroaggregate turnover and microaggregate formation: a mechanism for C sequestration under no-tillage agriculture. *Soil Biol. Biochem.* **32**, 2099–2103.
- Six J., Paustian K., Elliott E. T. and Combrink C. (2000b) Soil structure and organic matter: I. Distribution of aggregate-size classes and aggregate-associated carbon. *Soil Sci. Soc. Am. J.* **64**, 681–689.
- Six J., Conant R. T., Paul E. A. and Paustian K. (2002) Stabilization mechanisms of soil organic matter: implications for C-saturation of soils. *Plant Soil* **241**, 155–176.
- Six J. and Jastrow J. D. (2002) Organic matter turnover. In *Encyclopedia of Soil Science* (ed. R. Lal). Marcel Dekker, New York, pp. 936–942.
- Six J., Bossuyt H., Degryze S. and Deneff K. (2004) A history of research on the link between (micro)aggregates, soil biota, and soil organic matter dynamics. *Soil Tillage Res.* **79**, 7–31.
- Sokolowska Z., Hajnos M., Hoffmann C., Renger M. and Sokolowski S. (2001) Comparison of fractal dimensions of soils estimated from adsorption isotherms, mercury intrusion, and particle size distribution. *J. Plant Nutr. Soil Sci.* **164**, 591–599.
- Sollins P., Homann P. and Caldwell B. A. (1996) Stabilization and destabilization of soil organic matter: mechanisms and controls. *Geoderma* **74**, 65–105.
- Stacey M. H. (1988) A comparison of nitrogen adsorption, small angle neutron scattering and TEM techniques for characterization of mesoporous oxides. In *Characterization of Porous Solids* (eds. K. K. Unger, J. Rouquerol, K. S. W. Sing and H. Kral). Elsevier, Amsterdam, pp. 55–65.
- Tisdall J. M. (1996) Formation of soil aggregates and accumulation of soil organic matter. In *Structure and Organic Matter Storage in Agricultural Soils* (eds. M. R. Carter and B. A. Stewart). CRC Press, pp. 57–96.
- Tisdall J. M. and Oades J. M. (1982) Organic matter and water stable aggregates in soils. *J. Soil Sci.* **32**, 141–163.
- Tombacz E., Szekeres M., Baranyi L. and Micheli E. (1998) Surface modification of clay minerals by organic polyions. *Colloids Surf. A Physicochem. Eng. Aspects* **141**, 379–384.
- Venkatraman A., Boateng A. A., Fan L. T. and Walawender W. P. (1996) Surface fractality of wood charcoals through small-angle X-ray scattering. *AIChE J.* **42**, 2014–2024.
- Vetter Y. A., Deming J. W., Jumars P. A. and Krieger-Brockett B. B. (1998) A predictive model of bacterial foraging by means of freely released extracellular enzymes. *Microb. Ecol.* **36**, 75–92.
- Zhu Y., Fox R. H. and Toth J. D. (2002) Leachate collection efficiency of zero-tension pan and passive capillary fiberglass wick lysimeters. *Soil Sci. Soc. Am. J.* **66**, 37–43.
- Zhuang J., McCarthy J. F., Perfect E., Mayer L. M. and Jastrow J. D. (2008) Soil water hysteresis in water-stable microaggregates as affected by organic matter. *Soil Sci. Soc. Am. J.* **72**, 212–220.
- Zimmerman A. R., Goyne K. W., Chorover J., Komarneni S. and Brantley S. L. (2004) Mineral mesopore effects on nitrogenous organic matter adsorption. *Org. Geochem.* **35**, 355–375.

Associate editor: Donald L. Sparks